ANTC
Airbus Noise Technology Centre

UNIVERSITY OF Southampton

# Final Publishable Summary Report

# CLFCWTE

Researcher: Dr. Z. Cai

Investigators: Professor X. Zhang and Dr. D. Angland

Project title: Development of a Closed Loop Flow Control Algorithm for Wing Trailing Edge Flow Control Including Experimental Validation in Two Low Speed Wind Tunnel Tests

Date of Issue: February, 2014

UNIVERSITY OF SOUTHAMPTON

FACULTY OF ENGINEERING AND THE ENVIRONMENT

## ABSTRACT

The final report contains the results from the two experimental investigations that were conducted into a pre-modelled and adaptive control strategies. The primary results are from the pre-tests in WP5 and the mid-scale tests in WP6 (Task 6.2 and Task 6.3). This final report also includes the results from the second wind tunnel campaign (Task 6.3) that was conducted in Q3 2013, that were not included in the previous deliverables.

In this work, active flow control using pulsed air jets was investigated in order to delay flow separation on a two-element high-lift wing. The method was validated experimentally. A novel iterative learning control (ILC) algorithm was developed that uses position based pressure measurements to update the actuation. The method was experimentally tested on a wing model in a 0.9 m $\times$ 0.6 m wind tunnel initially and then the R. J. Mitchell wind tunnel at the University of Southampton. Compressed air and fast switching solenoid valves were used as actuators to excite the flow and the pressure distribution around the chord of the wing was measured as a feedback control signal for the ILC controller. Experimental results showed that the actuation was able to delay the separation and increase the overall lift by approximately 15% to 20%. By using the ILC algorithms, the controller was able to track the target lift and using the optimum control algorithm with an extended reference, the controller was able to maximize the lift enhancement. In the second wind tunnel test session, open loop tests were completed to generate data which was used to create a system model. A two-dimensional model function was then fitted using locally weighted scatter-plot smoothing and the model was applied in a model based iterative learning optimization algorithm. Wind tunnel experimental results showed that the method was able to optimise the performance with two variables and an overall lift enhancement of approximately 20% could be achieved.

# Contents

# List of Figures

# List of Tables

# Introduction

Smart Fixed Wing Aircraft (SFWA) aims to develop and test passive and active flow control technologies to improve the high lift performance of a wing. The technology will be used to help achieve the ACARE 2020 vision [1]. SFWA will work towards the reducing the emissions by 20% and the noise by 5-10dB. Pollution and the reduction in $CO_2$ emissions are also both politically and regulatory important issues.

In this research, the use of pulsed blowing will be used to delay separation, thereby increasing the performance of the high-lift system. The wind tunnel test model used in the research project was the DLR F15 high-lift model. Firstly, a small scaled model was built to test the effectiveness of the actuation. Secondly, a mid-scale model was used in two test sessions that took place in the R. J. Mitchell wind tunnel at University of Southampton. An iterative learning control (ILC) algorithm with novel positional based measurement setup is introduced in this application in order to find the optimum control input after the open loop control tests.

Iterative learning control (ILC) is a technique for controlling systems operating in a repetitive (or pass-to-pass) mode with the requirement that a reference trajectory $r(t)$ defined over a finite interval $0 \leq t \leq T$ is followed to a high precision. Motivated by human learning activities, it uses the tracking error information measured from previous trials to update the control input for the next iteration, and by repeating this iteratively, a perfect or desired control input can be learnt. Examples include robotic manipulators that are required to repeat a given task, chemical batch processes or, more generally, the class of tracking systems. Since the original work of [2], the general area of ILC has been the subject of intense research effort. Initial sources for the literature are the survey paper by [3] and [4] categorises and summarises a large number of ILC algorithms. Since the basic ILC algorithms do not need any information of the plant model it is suited to aerodynamic flow control where the plant model is very challenging to describe as it is an inherently non-linear system.

Until now, there are very few attempts of applying ILC to aerodynamic or active flow control problems. In this study, a novel position based iterative learning control algorithm was employed, which uses the surface pressures measured around the wing and flap surfaces to update the actuation, in order to maximise the improvement of lift and delay boundary layer separation.

# Pre-tests with A Small Scale High-lift Model

This section contains the results obtained primarily from Task 2.2, Task 3.3, Task 5.2 and Task 5.4 as part of the parametric study, pre-tests and closed loop flow control algorithm development before their implementation on the mid-scale F15 model.

## 2.1 Experimental Facilities

### 2.1.1 Wind tunnel

The initial concept proof experiments were conducted in the University of Southampton's 0.9 m $\times$ 0.6 m low speed wind tunnel. The tunnel has an open loop circuit with a closed test section of 4 m in length. The freestream turbulence was less than 0.2 % at the maximum tunnel speed of 25 m/s used in these experiments. The baseline test conditions were defined as a freestream velocity of 20 m/s, corresponding to a Reynolds number of $5.5 \times 10^5$ based on the chord of the retracted configuration. The exact separation on the flap is sensitive to how the flow is tripped to force transition from a laminar boundary layer to a turbulent boundary layer. In order to obtain the correct flow conditions, the boundary layer was tripped to ensure the boundary layer was turbulent before it separated from the flap.

### 2.1.2 High lift wing model

The wing model was a two-element high-lift configuration consisting of a main element and a trailing edge flap. It is an 80% scaled version of the DLR F15 wing model [5]. The chord length in clean cruise condition is $c_m = 0.445$ m and the span is 0.6 m. Figure 3.2 shows the diagram of the wing model mounted in the wind tunnel as well as the dimensions. A set of holes with 2 degrees between each other were placed on both end plates enabling the angle of attack to be varied from 0 to 12 degrees. A set of adjustable brackets were made to enable tuning of the flap gap and overlap (see Figure 3.2(c) for definition) as the flap gap and overlap are crucial parameters in determining the position of flow separation on the flap.

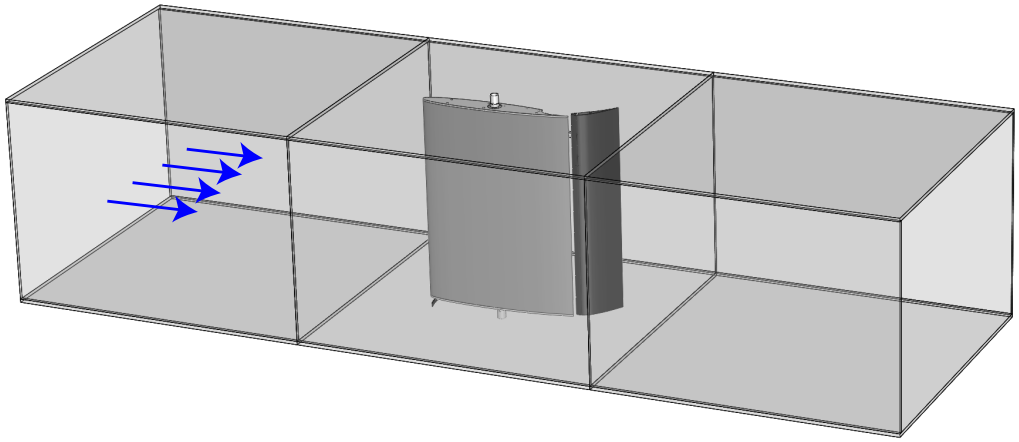

(a)

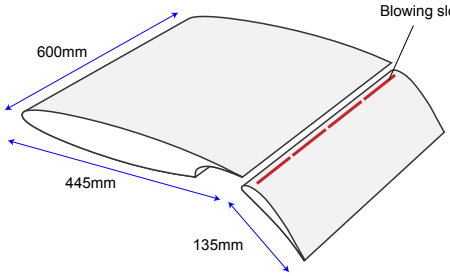


(b)

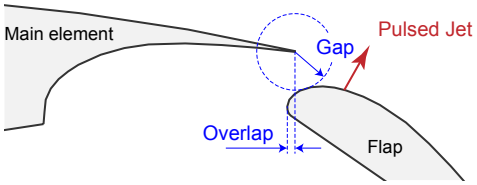


(c)

Figure 2.1: (a) Wing model mounted in wind tunnel, (b) Wing model dimension, (c) Definition of the gap and overlap.

### 2.1.3 Actuators

There were 4 actuator segments designed and positioned along the span of the wing model. Each segment was approximately 0.12 m wide and includes a FESTO MHE2 series fast switching solenoid valve and a chamber. All segments were supplied with high pressure compressed air. The valves were supplied with a high frequency periodic pulse signal at the desired frequency and the duty cycle of the pulse can be tuned as a control input. The position of the excitation was located at $x_e/c_f = 0.1$ on the suction side of the flap. The jet direction was normal to the surface. Figure 2.2(a) shows the actuator setup inside the model. Because of the limited space in the flap, the fast switching valves were mounted inside the main element and connected to the chamber inside the flap. Since the connecting tube was short, the frequency and strength of pulsed jet could be maintained.

It was found experimentally that tuning the duty cycle (pulse width) of the switching pulses for the valves was able to change the effectiveness of the flow excitation. To maximise the improvement, feedback control was needed with tuning of the duty cycle as the control input. Figure 2.2(b) shows the pulses which were fed into the actuators and the response which was measured by using hot wire anemometry at the exit of a blowing slot.

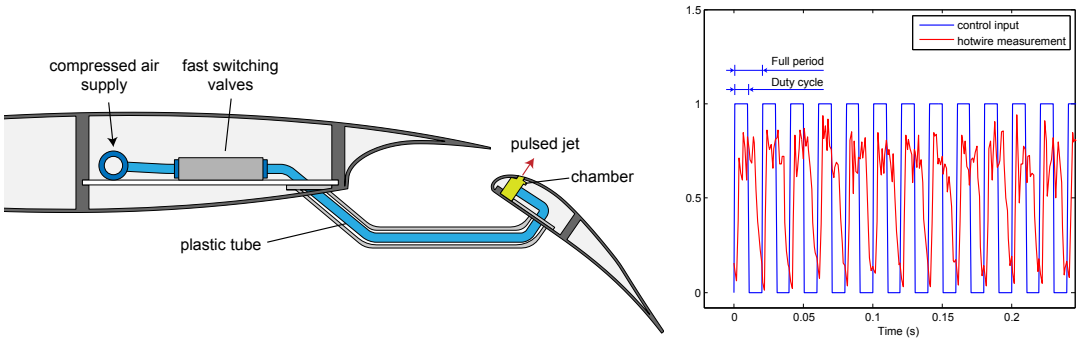


(a) (b)

Figure 2.2: (a) Diagrams of the actuator setup inside the wing model. (b) Actuator input and output measured by a hotwire.

### 2.1.4 Pressure scanner

A total of 20 pressure taps were placed on the suction and pressure surfaces of the flap on the centre line of the span. The pressure taps were connected to a Scanivalve ZOC33 pressure scanner using tubes with an inner diameter of 1.98 mm. The length of the connecting tubes were less than 1 m long in order to maximise the response that the pressure scanner could obtain. The pressure scanner had a very high scanning rate of 40 kHz, so over the 20 channels used, the maximum scanning frequency could potentially be 2 kHz. In the tests, a scanning frequency of 100 Hz was used to ensure that there were multiple points that could be measured and averaged for better quality.

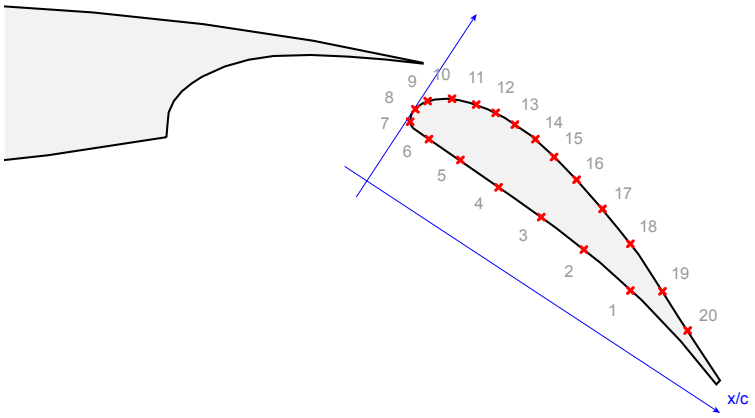


Figure 2.3: Pressure tap positions on the flap surface.

In the study, two-dimensional flow control was considered as the pressure measurements were taken from the centre line of the wing model span. All 4 span-wise actuators were given the same control input.

### 2.1.5 Experimental setups

A number of tests were conducted in the wind tunnel. The control of actuators and pressure measurements was achieved by a dSPACE (DS1006) system with a multi-channel A/D and D/A boards. Table 3.1 shows the configuration that was used to obtain all the experimental results.

Table 2.1: Configuration used in the pre-test experiments

| **Parameter** | **Value** |
|---|---|
| Free stream velocity | 20 m/s |
| Angle of attack $\alpha$ | 2° |
| Flap deflection $\delta_f$ | 40° |
| Flap gap | 13.0 mm |
| Flap overlap | 3.5 mm |
| Blowing pressure | 4 bar |
| Blowing frequency | 20 Hz |

Figure 2.4 shows the overall structure of the system and controller. An air compressor is attached to the supply tube and pressure measurement and actuation are controlled by dSPACE system.

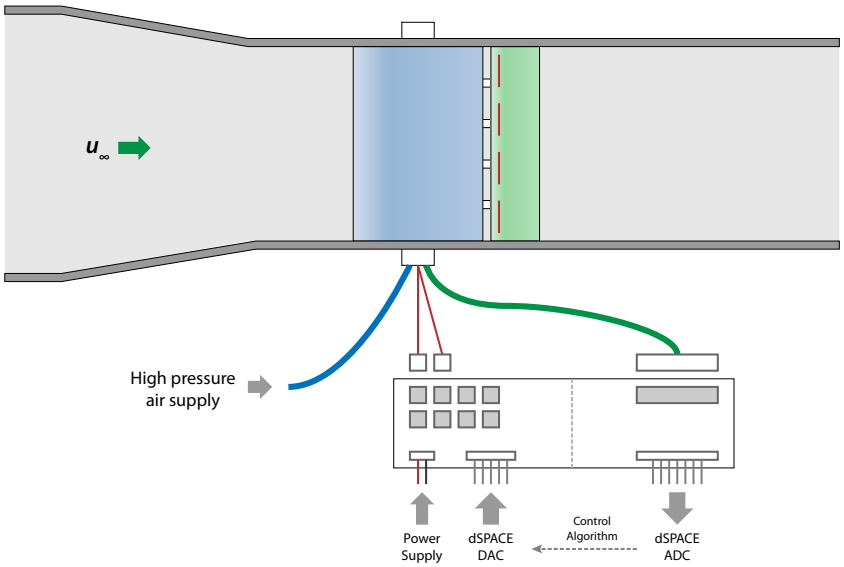


(a)

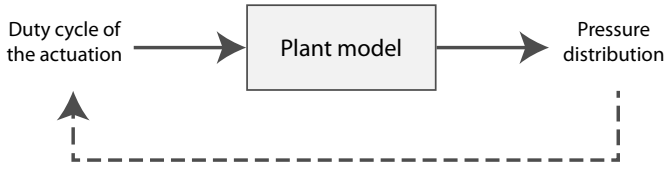


(b)

Figure 2.4: Overall structure of the control system

## 2.2 Open Loop Control

Open loop studies were conducted to test the controller with a series of fixed control inputs. The open loop tests were conducted in order to make sure that lift improvement could be obtained and also to provide a reference for the ILC algorithm. Each test with one fixed control input lasted a duration of 10 seconds in order to ensure enough output data was measured and all the pressure measurements were averaged. Figure 2.5 shows a series of pressure distributions, ranging from a duty cycle of 10% to 80%. The improvement in lift can be seen by comparison to the results without any actuation. The flow separation occurred at around 20% of flap chord and it was shifted downstream towards the trailing edge of the flap. Petz and Nitsche [6] and Haucke et al. [7] demonstrated that the jet frequency had little influence on the performance of actuation. Therefore in the current study only one frequency of excitation was tested.

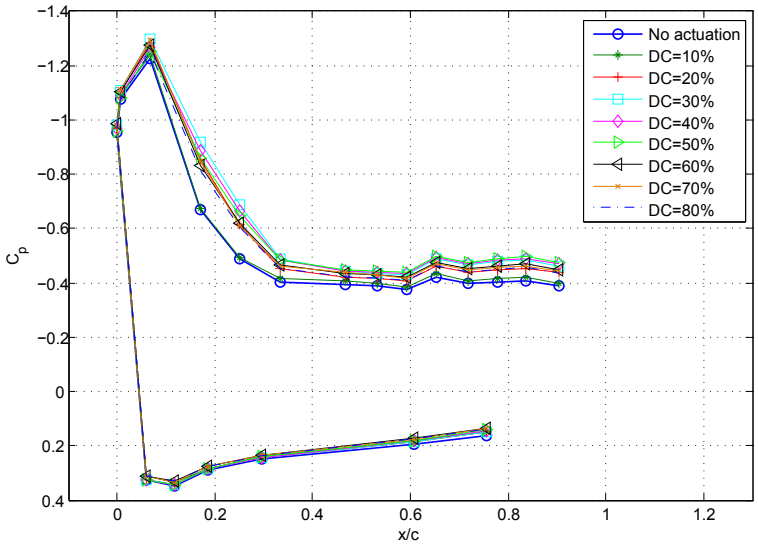


Figure 2.5: Pressure measurements from open loop tests.

The relationship between the lift improvement and the control input is shown in Figure 2.6. There was an optimum duty cycle between 20% and 30%. The aim of the ILC controller was to find the optimum control input accurately and maintain the performance even with varying freestream conditions.

## 2.3 Iterative Learning Control

### 2.3.1 Position based ILC

The fundamental algorithm of iterative learning control given by [2] was a continuous time derivative type (D-type) ILC which uses the derivatives of the tracking error with a

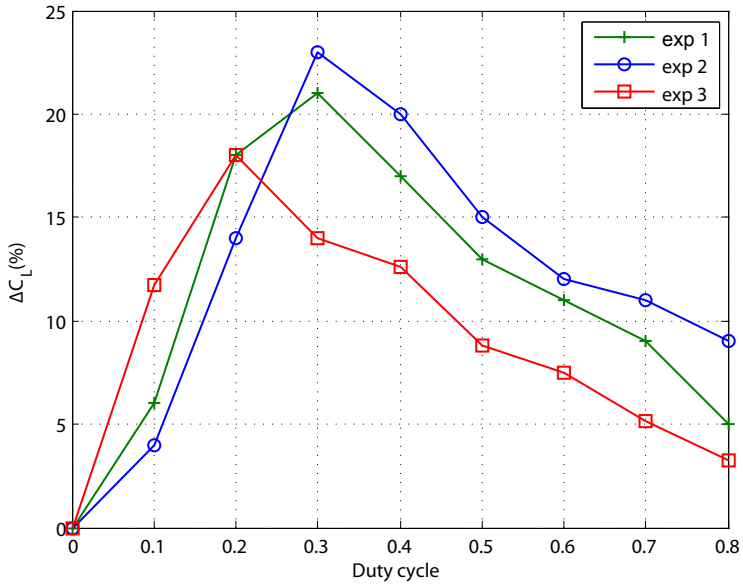


Figure 2.6: Improvement as a function of duty cycle.

learning gain to update control input. It can be written as:

$$u_{k+1}(t) = u_k(t) + L\dot{e}_k(t), 0 \leq t \leq T \tag{2.1}$$

where $k$ denotes the iteration number (or trial number), $u_k(t)$ is the control input for the $k^{th}$ iteration. $L$ can be a simple gain or a vector or a matrix depending on different sub algorithms. $e_k(t)$ is the tracking error of the $k^{th}$ iteration and

$$e_k(t) = r(t) - y_k(t)$$

where $y_k(t)$ denotes the measured output of $k^{th}$ iteration. Theoretically, $e_k(t)$ will converge to zero where the trial number $k$ approaches infinity, and at the mean time $u_k(t)$ converges to a constant value or vector $u_d(t)$, the ideally desired input for the plant to produce the reference output $r(t)$. That is also the numerical solution to the plant model with the given reference if it can be described by a mathematical equation. The algorithm is later simplified into a proportional type (P-type) ILC by [8] because the derivatives sometimes bring uncertainty and would make the learning process unstable especially with the discrete measurement when there is noise inherently in the signal.

$$u_{k+1}(t) = u_k(t) + Le_k(t) \tag{2.2}$$

Figure 2.7 shows the block diagram of the normal ILC process.

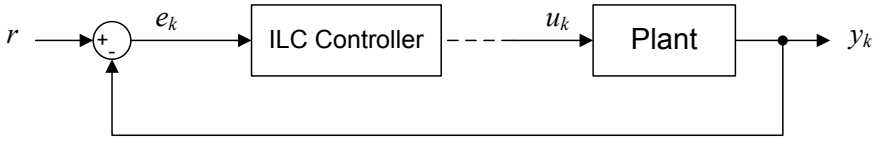


Figure 2.7: Block diagram of basic ILC algorithm

Here $t$ is the time step and $T$ represents the finite time interval. All signals in the setup are time based or sample based in the case of discrete time. Now the time step $t$ can be replaced with $p$ — a position index of measurement alongside chord length of the flap (as shown in Figure 3.5). Therefore within the trial, the controller will scan all the position and get the pressure measurement as plant output $y_k(p)$. The error $e_k(p)$ is still the difference between reference $r(p)$ and the output. Hence the ILC law will become:

$$u_{k+1}(p_u) = u_k(p_u) + Le_k(p_y) \tag{2.3}$$

where $p_u$ and $p_y$ are the positional indexes of the control input and output, respectively. Here it is not necessary for the control input to have one to one mapping with the output and tracking error. Since there is only one actuator placed along the chord length in this particular configuration, the norm of the error is used for the update of control input iteratively. Thus the ILC updating law can be written as:

$$u_{k+1} = u_k + L||e_k(p)|| \tag{2.4}$$

where $L$ is the learning gain and it can be tuned to alter the converge speed.

The measurement of one trial will collect all the static pressure data on the surface for a fix duration and at each point the measurements will be averaged. Therefore all the measurement should be a steady state measure of the flow behaviour. At this stage, no time dynamic is considered because the generation of turbulent flow is too random, so that time dynamic on a fix point is not useful and important for the controller to control the overall flow separation.

### 2.3.2 Reference signals

The reference signal is one of the essential conditions that ILC requires to perform. However, unlike the typical tracking control problem (e.g. robot arms trajectory control), the controller here is used to maximise the improvement of the actuation. From the experimental results of open loop control, it is known that at a certain duty cycle range, the improvement can be maximised. The maximum results from open loop tests can be used for the reference signal and an additional offset has been added on the top of the reference to ensure the controller is able to maximise the improvement. Figure 2.8 shows an illustration of the pressure measurement and the defined reference. In this case an extra algorithm is developed to enable the convergence

$$u_{k+1} = u_k + D_k \cdot L \cdot ||e_k(p)|| \tag{2.5}$$

where $D_k$ refers to the direction of learning at $k$th iteration, and

$$D_k = \begin{cases} D_{k-1}, ||y_k|| > ||y_{k-1}|| \\ -D_{k-1}, ||y_k|| < ||y_{k-1}|| \end{cases} \tag{2.6}$$

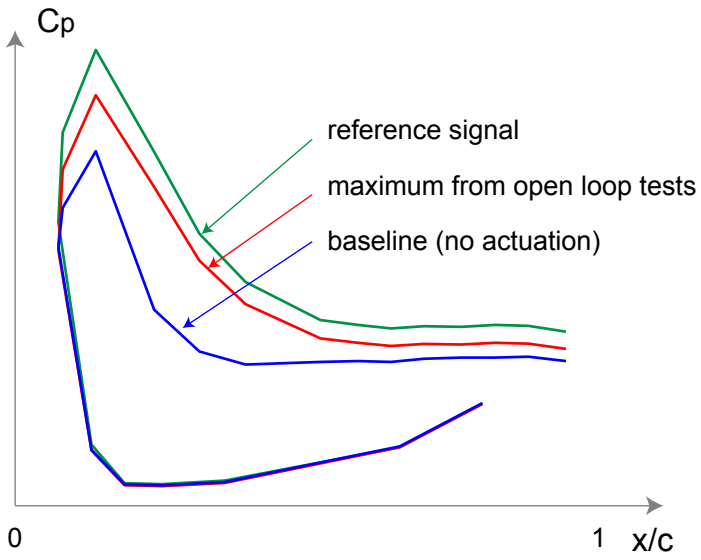


Figure 2.8: Reference signal defined by the maximum output from open loop tests.

where the initial direction $D_0 = 1$.

Since the reference $r$ is set to beyond the reach of plant output $y_k$ as

$$\lim_{k\to\infty} y_k < r$$

The computed error is not able to converge to zero.

$$\lim_{k\to\infty} e_k \to r - y_{max}$$

Therefore if the normal ILC setting in (2.1) or (2.2) was used, the learnt input would not be bounded with a fixed positive learning gain $L$ as

$$\lim_{k\to\infty} u_k = \lim_{k\to\infty} (u_{k-1} + L \cdot e_{k-1}) \to \infty$$

This means the control input will be unstable and no optimum input can be learnt to maximise the improvement.

The learning direction is defined in (2.6) because there exists an ideal input $u_d$ where the maximum output can be obtained. Initially the controller will make $u_k$ converge towards $u_d$. When the learnt input $u_k$ is greater than $u_d$, the output is going away from the optimal values, therefore the controller needs to change its direction. And with a carefully selected learning gain $L$, although the reference $r$ can be not reached, the output $y_k$ is converging towards the maximum value $y_{max}$.

### 2.3.3 Experimental results

The ILC controller was tested using a learning gain $L = 0.2$. The iteration length $T$ was set to 5 seconds in order to get enough data for accurate pressure measurements. Figure 2.9

shows the pressure measurement of 100 iterations in one set of results. Figure 2.10 shows the improvement along the iterations. Here the term $\Delta C_L$ is computed by integrating the pressure coefficients $C_P$ in each trial. The pressure distributions were significantly improved compared to the baseline without any actuation. At the $94^{th}$ and $95^{th}$ iterations there appeared to be some sudden flow separation, however, the controller reacted and recovered an optimum within 2 trials. After only 5-10 iterations, the improvement of lift could be maintained at between 10% - 15% for the remainder of the test except for the sudden change of separation. This demonstrated the performance and robustness of the ILC controller.

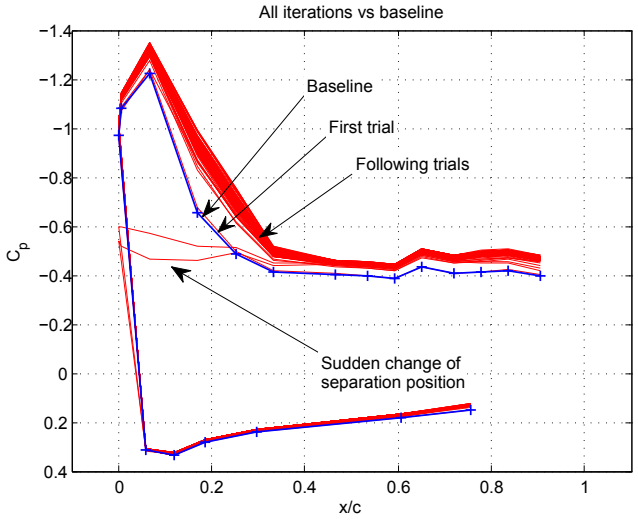


Figure 2.9: Pressure distribution of all 100 iterations in one experiment.

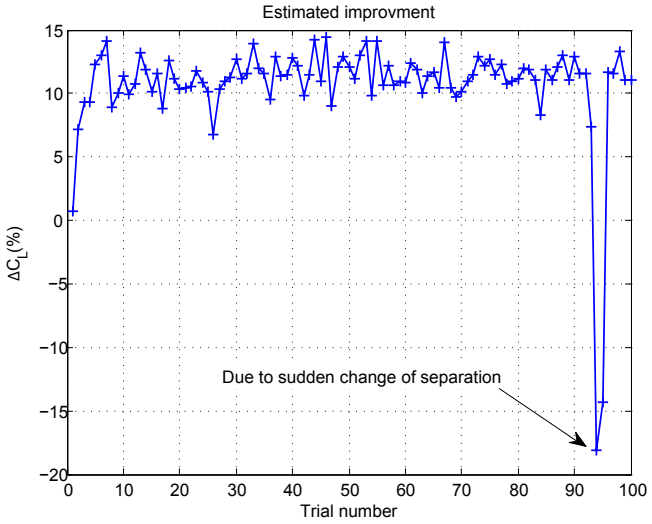


Figure 2.10: Improvement over 100 iterations in one experiment.

Figure 2.11 shows the recorded control inputs over all iterations. The learning process in the initial iterations is clearly visible. The benefit from the actuation is shown in Figure 2.12, where the best outputs are selected and overlapped. The best results from a series of tests are very similar even though some of the control parameters were different. Using

larger learning gain will not only increase the convergence speed but also the fluctuation of the input around the optimum value. Using smaller learning gains will slow down the learning progress. The trial length will affect on measurement accuracy as a shorter trial (e.g. $T = 2$ s) makes the controller respond faster but degrades the measurement accuracy.

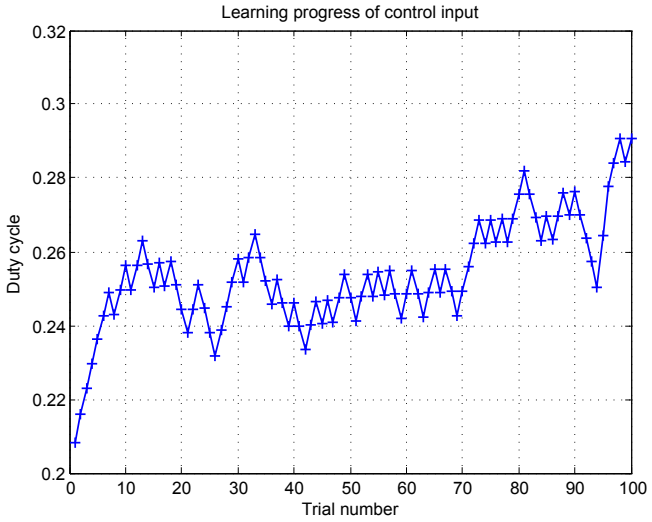


Figure 2.11: Control inputs evolution for all 100 iterations.

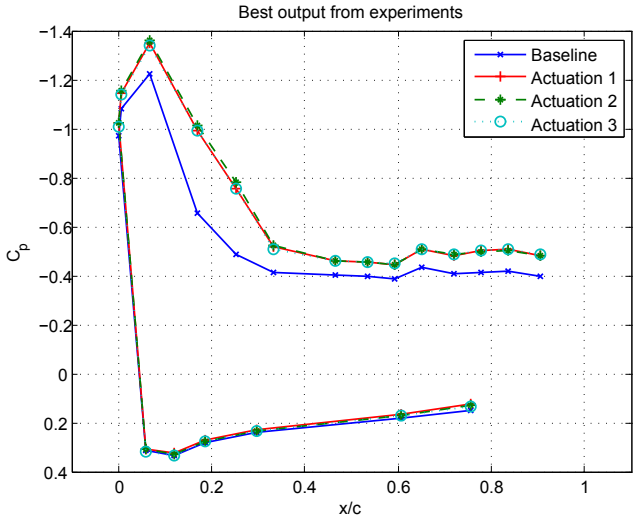


Figure 2.12: Benefit of the actuation.

Figure 2.13 shows the result taken when the trial length $T$ was set to 2 seconds. The trend of improvement is visible but the performance suffered from some large fluctuation. Making the trial length longer can certainly improve measurement accuracy however, the controller would respond slower. A comparison of the control input is shown in Figure 2.14 and with shorter trial length, the learning process appears to be not as stable as when the length was set to a larger value. The reason is within a short period of time, there was not enough data to get an accurate measurement of the pressure distribution. Also change of actuation sometimes requires a longer settling time for the flow to reattach or

change behaviour.

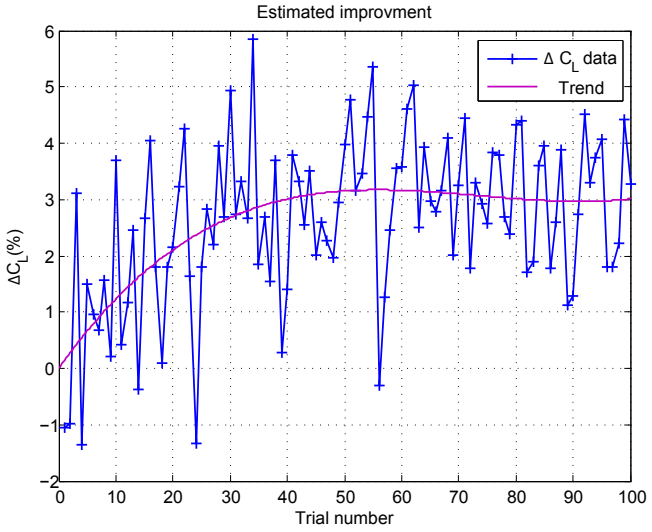


Figure 2.13: Improvement over 100 iteration ($T = 2$).

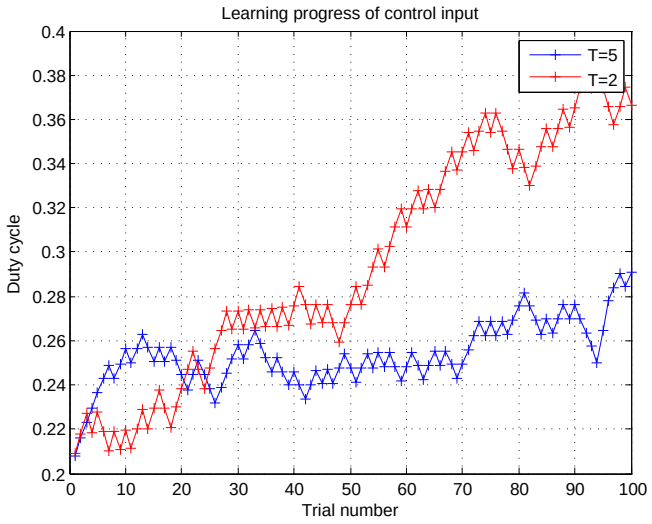


Figure 2.14: Comparison of the control input for different trial lengths.

# Mid-scale Test Model and Experimental Setup

## 3.1 High Lift Wing Model and Wind Tunnel

The wing model used here is a two-element high lift configuration consisting of a main element and a trailing edge flap. It is the mid-scale version of the DLR F15 wing model [5]. Figure 3.1 shows the assembly of the high lift wing model and the key dimensions and figures are listed in Table 3.1.

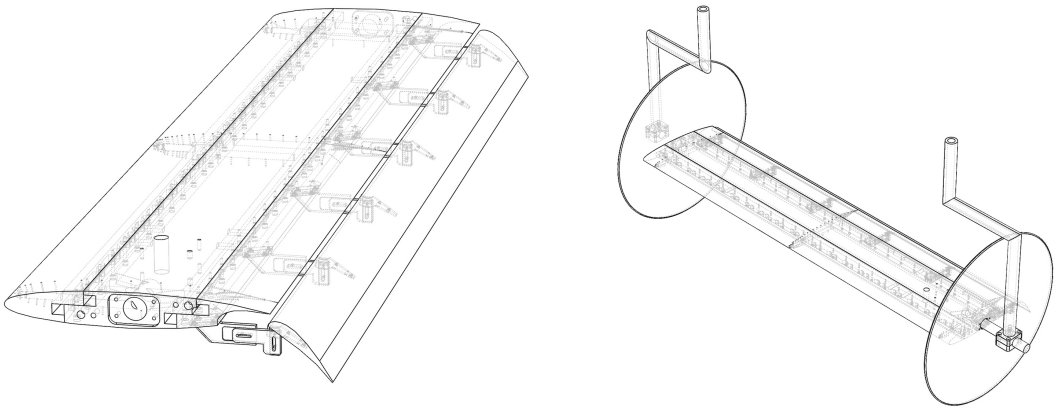

(a) Model assembly (b) Model with end plates

Figure 3.1: High lift wing model

Table 3.1: Configuration used in the wind tunnel tests

| **Parameter** | **Value** |
|---|---|
| Clean cruise chord length | 600 mm |
| Flap chord length | 168 mm |
| Flap deflection | 45° |
| Flap gap | 15.919 mm |
| Flap overlap | 3.303 mm |
| Wing span | 2371 mm |

Figure 3.2 shows the photos of the high lift model mounted in the R. J. Mitchell wind tunnel at University of Southampton. The R. J. Mitchell wind tunnel is a large and extensively equipped low-speed wind tunnel with a 3.6 m × 2.5 m (11× 8) working section, with a

moving ground and a maximum wind speed of 45 m/s with less than 0.2% turbulence. An air chiller was used to control airflow temperature to 19 °C. The Reynolds numbers for the free stream velocity of 25 m/s and 30 m/s are $0.99 \times 10^6$ and $1.19 \times 10^6$, respectively. In order to obtain the correct flow conditions, the boundary layer was tripped to ensure the boundary layer was turbulent before it separated from the flap. Tripping tapes were applied to the leading edge of both the main element and the flap.

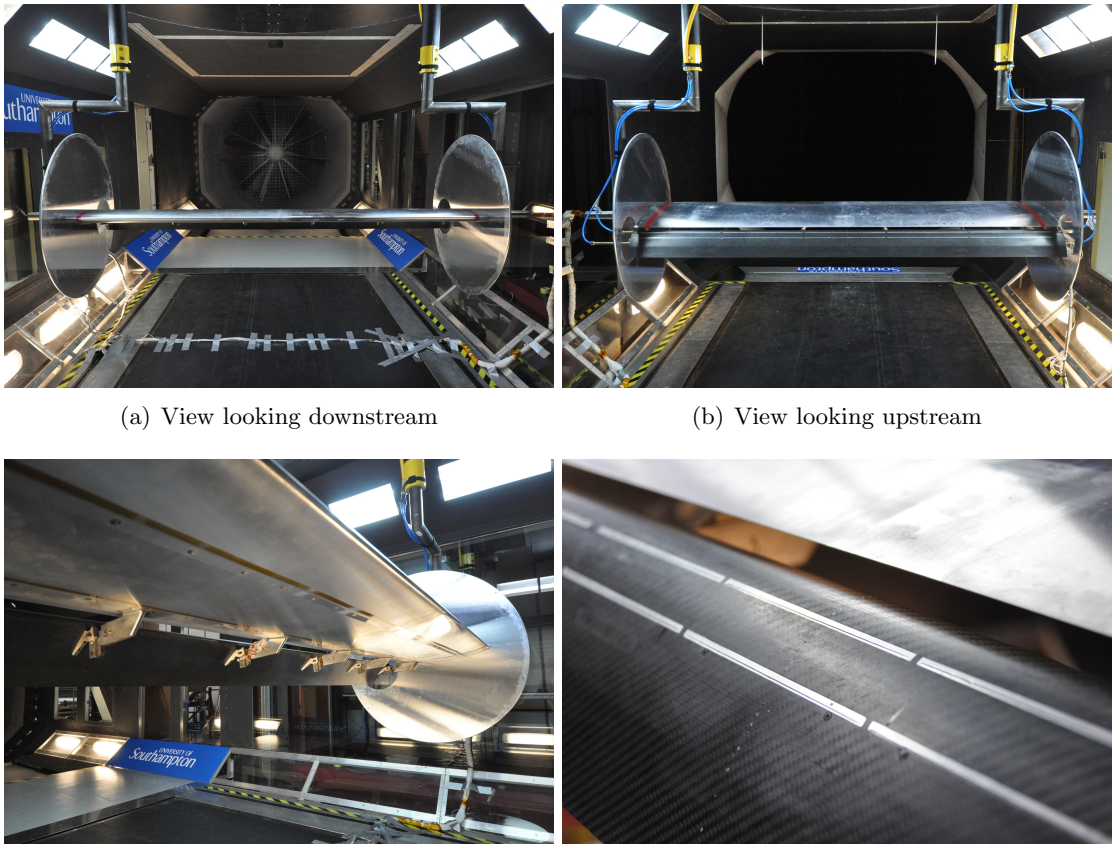

(a) View looking downstream

(b) View looking upstream

(c) Flap connection

(d) Actuators and pressure taps

Figure 3.2: High lift wing model mounted in the R. J. Mitchell wind tunnel

## 3.2 Actuators

### 3.2.1 Actuator designs

Figure 3.3 shows the assembly and side view of the actuator design within the flap. Two blowing slots were designed along the chord of the flap and positioned at 20% and 40% of the flap chord length, respectively. Span-wise, 15 actuators were designed in 5 sections for both slots. Each actuator includes a fast switching solenoid valve (FESTO MHJ9-QS-4-MF) and a chamber. The switching frequency of the valves is up to 1 kHz. Each valve has a maximum pressure limit of 6 bar and has a maximum flow rate of 100 l/min. The valves are connected to 4 supply tubes that supply the compressed air. The valves were supplied with a high frequency periodic pulse signal at the desired frequency and the duty cycle of

the pulse can be tuned as a control input. The jet direction is 30 degree with respect to the surface tangent line. Each actuator is 142 mm long and the slot width is 0.5 mm.

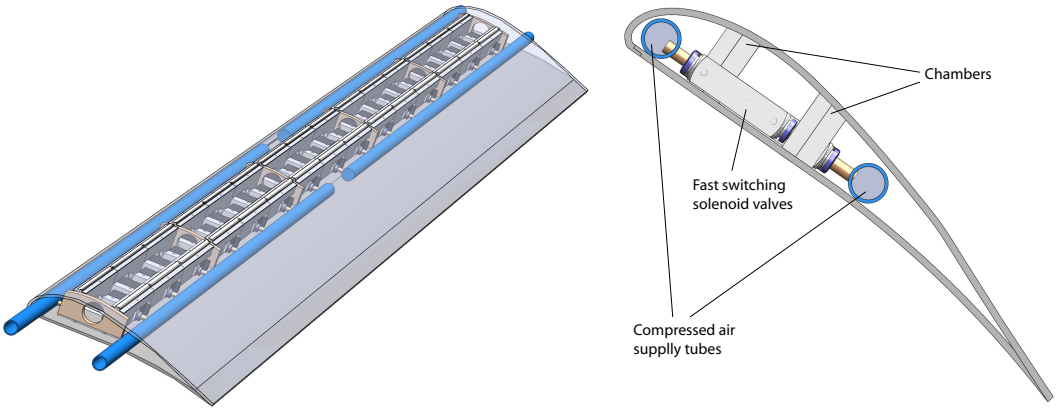


(a) Flap assembly (b) Flap side view

Figure 3.3: Actuators in the flap

### 3.2.2 Hot wire tests

The exit velocity of the jet from a single actuator was measured by using hot wire anemometry. Figure 3.4(a) shows the velocity measure of a jet pulse of 10 Hz with air supply at a pressure of 5 bar. The instantaneous jet velocity can reach around 20 m/s. The mean velocities of jet using different pressures and frequencies were recorded and are shown in Figure 3.4(b). The bigger the supply pressure was, the higher the jet velocity could reach. The change of frequency had less influence to the mean velocity of the jet.

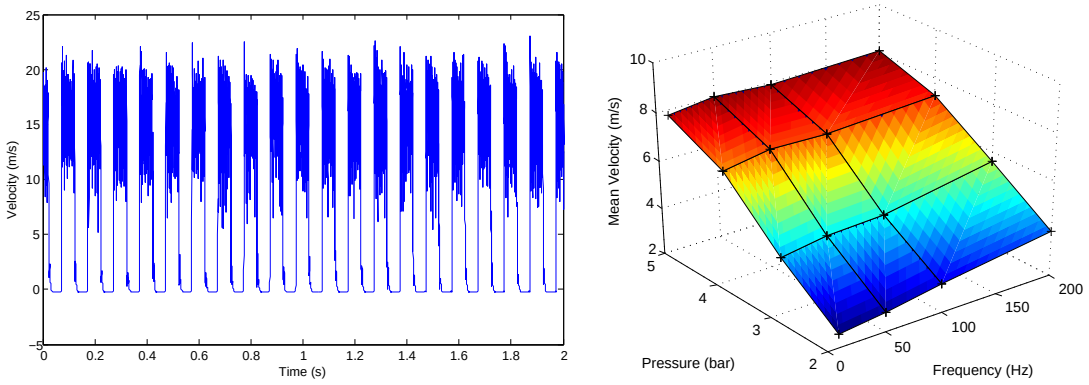


(a) (b)

Figure 3.4: Hotwire velocity measurements

## 3.3 Pressure measurement

In the centre of the span, there are 51 pressure taps on the main elements and 31 on the flap as shown in Figure 3.5. The pressure taps were connected to two Scanivavle ZOC33-64px pressure scanners.

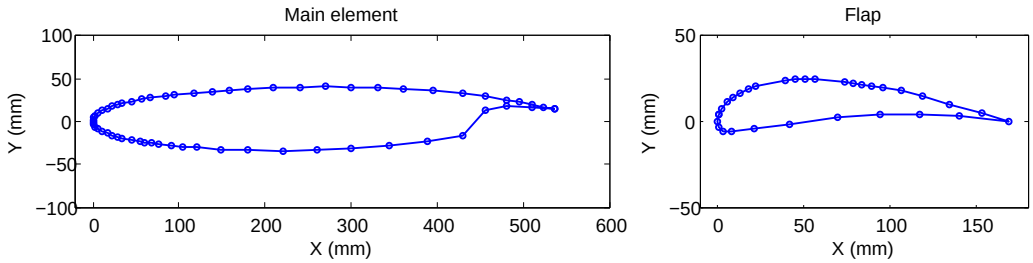


Figure 3.5: Positions of the pressure taps

## 3.4 Control system and hardware

The system was controlled by a program running on a PC with a dSPACE DS1006 system. Measurement were taken by using a DS2003 A/D convertor and control signals were sent by a DS2103 D/A convertor. The system program was developed by using Matlab/Simulink with integrated dSPACE I/O blocks. The sampling frequency for all the tests conducted was $10^4$ Hz. Figure 3.6 shows a screenshot of the control system software.

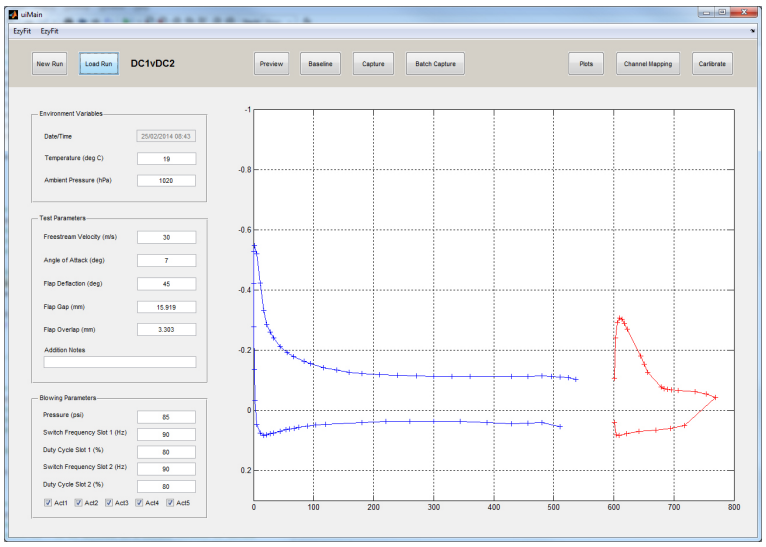


Figure 3.6: The screenshot of the control system software

# Wind Tunnel Experimental Results

## 4.1 First wind tunnel tests

This section contains the results of the first wind tunnel test on the mid-scale F15 model (Task 6.2).

### 4.1.1 Open loop tests

The open loop tests tested the controller with fixed control inputs. Each test lasted a duration of 10 seconds in order to ensure enough data will be measured and all the pressure measurement can be averaged. A number of parameters were varied, including the angle of attack, the actuation frequency, the duty cycle, the phase delay and the pressure.

#### Angle of attack

The angle of attack was varied and 9 values were set until the wing was stalled. Figure 4.1 shows all the pressure measurements when different angle of attacks were set. At 11° the wing was stalled and it appeared that there was little flow separation on the flap.

Figure 4.2 shows the calculated lift coefficients of angles of attack from $-1°$ to $11°$ for different cases: the baseline without any actuation, actuation on slot 1 only, slot 2 only and on both. The improvement of lift is obvious until the wing was stalled. The actuation had no effect when there was no flow separation on the flap. The results also indicate that the actuation on slot 2 had greater impact on the improvement of the performance than using slot 1. Using both at the same time appeared to be the superior. The following test results were taken using the wing model fixed at $AoA = 7°$.

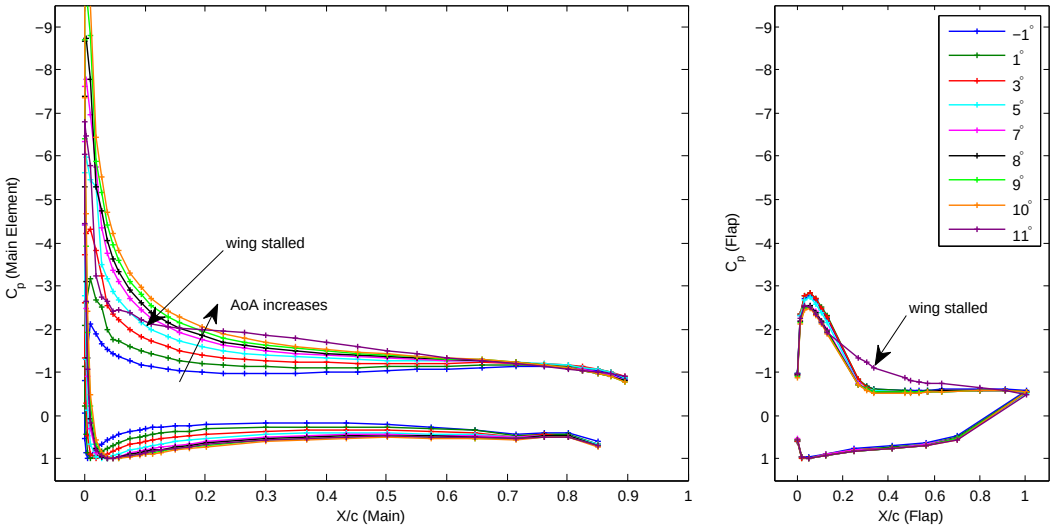


Figure 4.1: Pressure distribution of different angles of attack

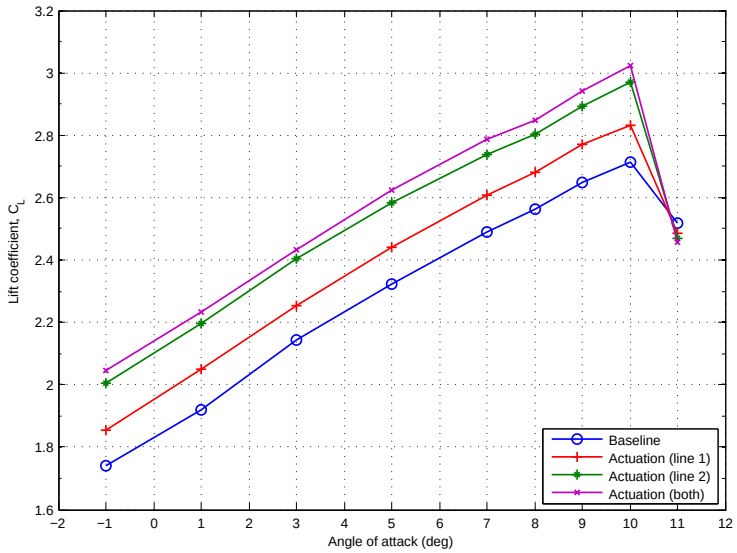


Figure 4.2: Lift coefficients of different angles of attack

### Frequency

The frequency of the pulse can be tuned via the pulse generator in the control program. Figure 4.3 shows the pressure distribution results using different excitation frequencies. The actuation managed to improve the lift for all frequencies tested and using different frequencies had a different effect on the performance. All the tests were conducted with a duty cycle of 50%.

Figure 4.4 shows the improvement of the lift based on the pressure measurements. The result indicates that the frequency 60 Hz has resulted in the superior performances. Therefore, the actuation frequency of 60 Hz was used in the other open loop or close loop tests.

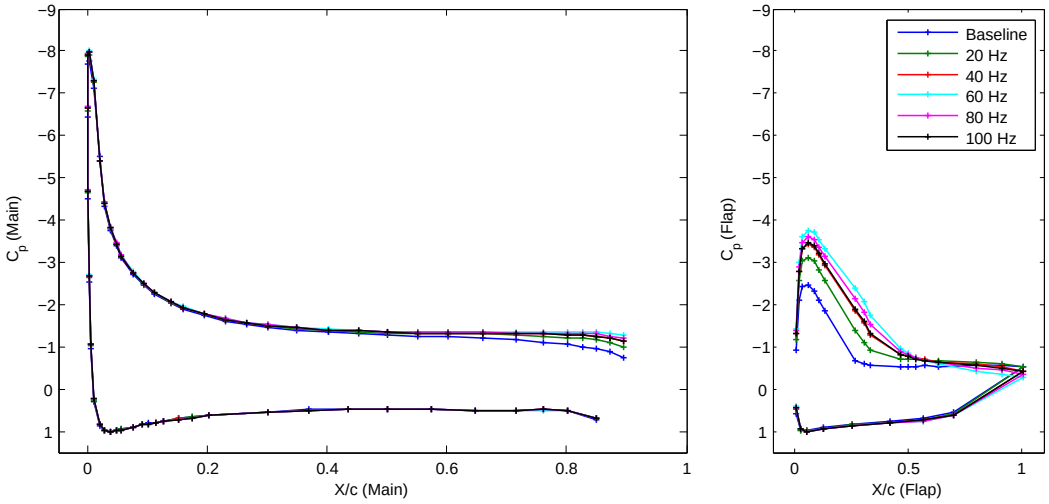


Figure 4.3: Effect of changing actuation frequency (slot 2)

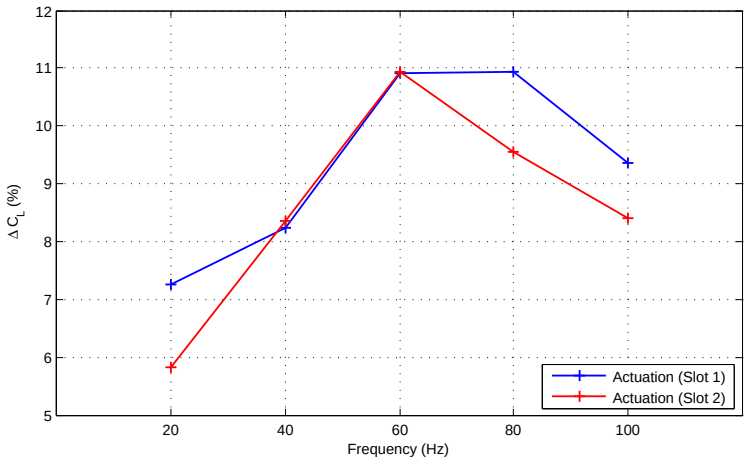


Figure 4.4: Improvement in lift using different actuation frequencies

### Duty cycle

The duty cycle is another parameter that can be tuned in the pulsed jet actuation. It was proved to be the most effective part by previous experiments. The tests used fixed duty cycle as control input and the results were collected. The results were also used to generate the set points and the reference for the closed loop control. A simple linear model could be fitted to for any model based control algorithms by using the input and output data mapping. Most of the tests were conducted when the AoA was set to 7°. Figure 4.5 shows the pressure distribution using different duty cycles as control input for both slots.

Figure 4.6 shows the lift improvement of using different duty cycles at different position. It verified that the second actuation slot at 40% flap chord length had greater impact on the performance. The optimal duty cycle could be found between 50% and 80%.

Figure 4.7 shows the lift improvement of using different duty cycles for different actuation frequencies. This also verifies that the frequency of 60 Hz could produce better overall

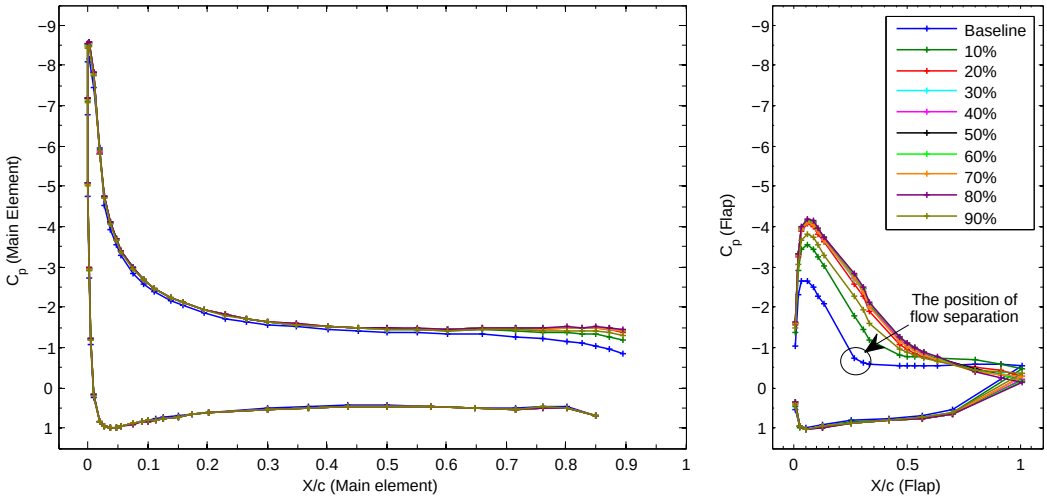


Figure 4.5: Pressure distribution of using different duty cycles

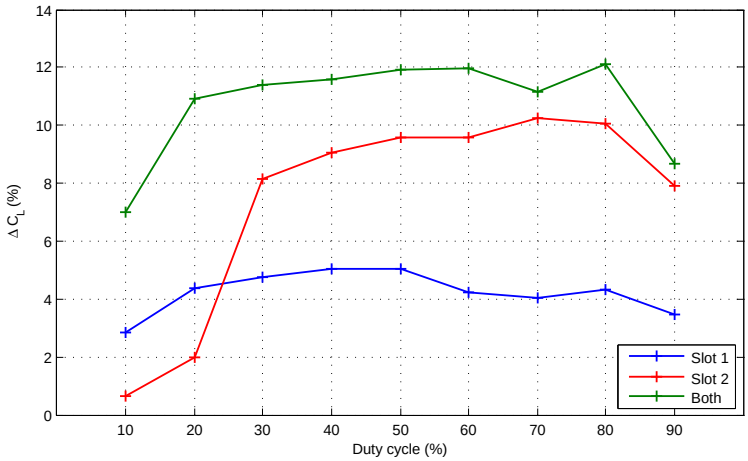


Figure 4.6: Improvement of using different duty cycles at different position

performance.

### Compressed air pressure

The pressure of the compressed air feed was tuned and the results of performance were recorded. Figure 4.8 shows the pressure distribution using different pressures of compress air feed for the actuation. The higher the pressure was, the better the lift improvement can achieve. The pressure reading from the compressor and the reading at the model end just before the valves were both recorded. There was a slight pressure drop due to the structure and connection of the system. When the compressor output was set to 90 psi (6.2 bar), the reading from the model end showed 84 psi (5.8 bar). Since the solenoid valves used here have a limit of pressure supply at 87 psi (6 bar), most of the following tests were conducted using 90 psi as the air feed pressure.

Figure 4.9 shows the results of using different duty cycles and pressures.

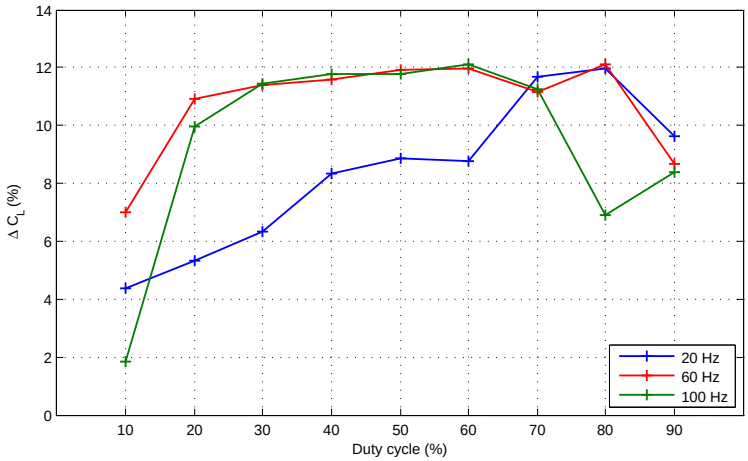


Figure 4.7: Improvement of using different duty cycles for different frequencies

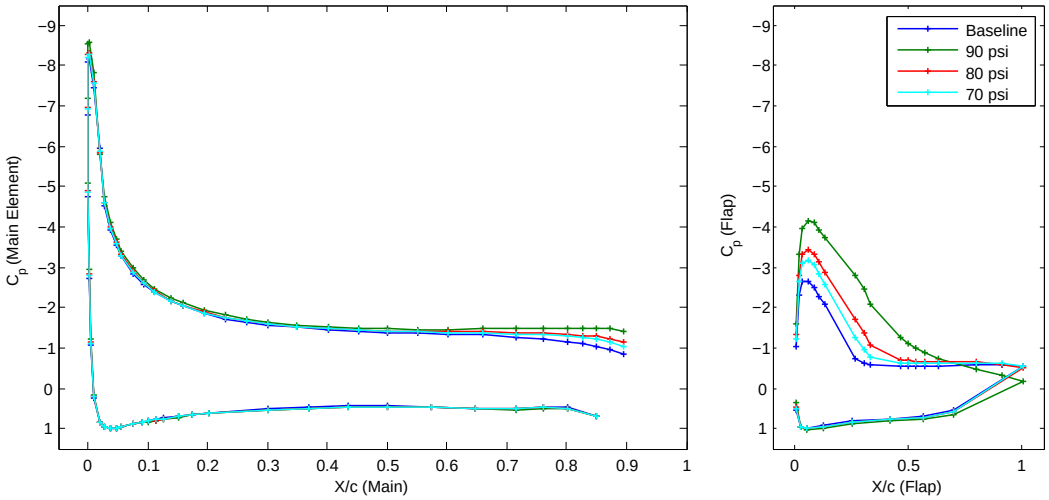


Figure 4.8: Pressure distribution using different pressures

### Phase delay

Since there were 2 actuator slots along the chord (at 20% and 40% of the flap chord length), they can be activated simultaneously or separately. A phase delay was applied to the second actuator slot. At percentage of period was used as the value of phase delay. Figure 4.10 shows the pressure distribution using different phase delay values. It shows that using a phase delay at about half of the period produced superior results, which means the actuation could be activated alternatively rather than simultaneously.

Figure 4.11 shows the lift improvement using different phase delays at different freestream velocities. In the figure, a delay value set to zero means the actuation was activated simultaneously. It shows that using a phase delay of about half of the excitation period could help improving the performance especially when simultaneous actuation was performance less effectively at higher freestream velocities.

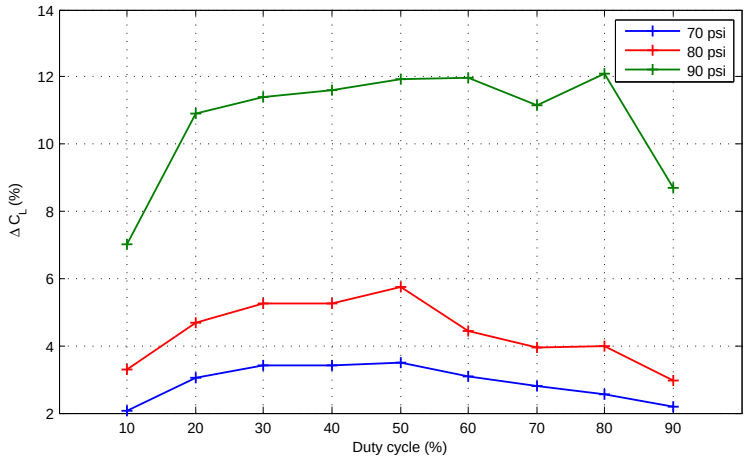


Figure 4.9: Improvement of using different duty cycles for different pressures

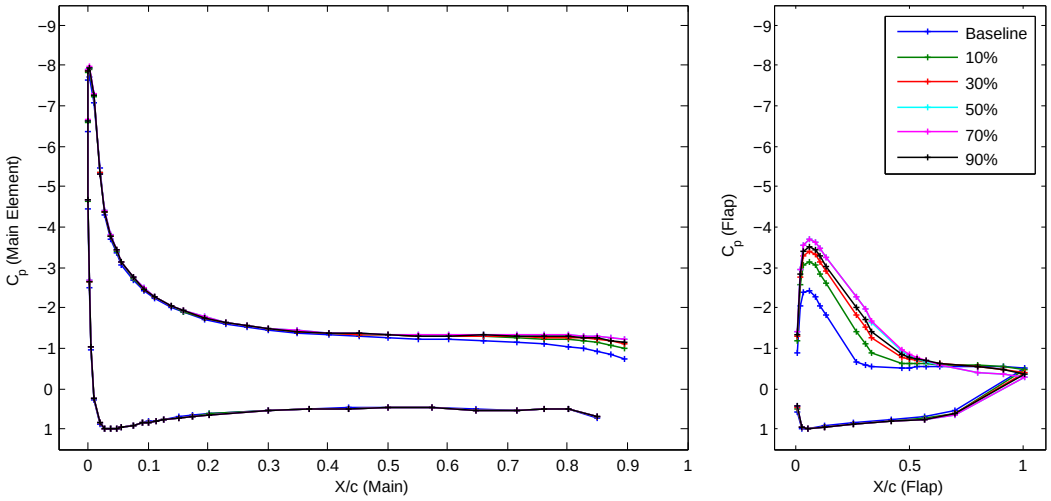


Figure 4.10: Pressure distribution of using different phase delays (% of period)

### 4.1.2 Closed loop control

Closed loop control strategy was designed and tested in previous experiments including using some conventional feedback control methods e.g. PID controller or PI controller, and an advanced iterative learning controller. The controllers used the pressure distribution as the feedback. The control input used in the tests was the duty cycle of the actuation.

#### PID/PI controller

Basic three term PID controller was tested. A sample frequency of 1 Hz was set for the controller but within the period of one second, the measurement signal was still sampled at a high frequency but the measurements were averaged. The control input at each control sample was:

$$u(t) = K_p e(t) + K_i \int_0^t e(\tau)d\tau + K_d \frac{d}{dt} e(t) \tag{4.1}$$

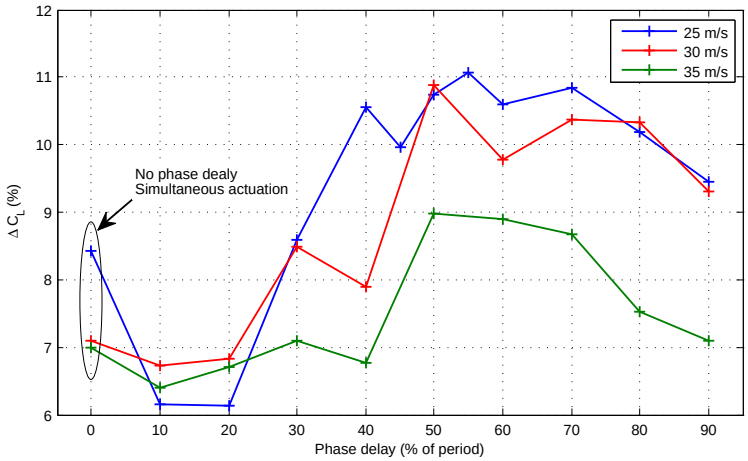


Figure 4.11: Improvement of using different phase delay at different freestream velocities

where $K_p, K_i, K_d$ were the proportional, integral and derivative gains, respectively. The error $e(t) = SP - y(t)$ was the difference between the set point and the output. As in this case, everything was discrete, the integration and derivative were computed using discrete methods.

A set point from the open loop results was used for the controller. Figure 4.12 shows the control input and lift improvement of using the PID controller. The improvement converged to the set point which was selected from the open loop test results using the a duty cycle of 30%.

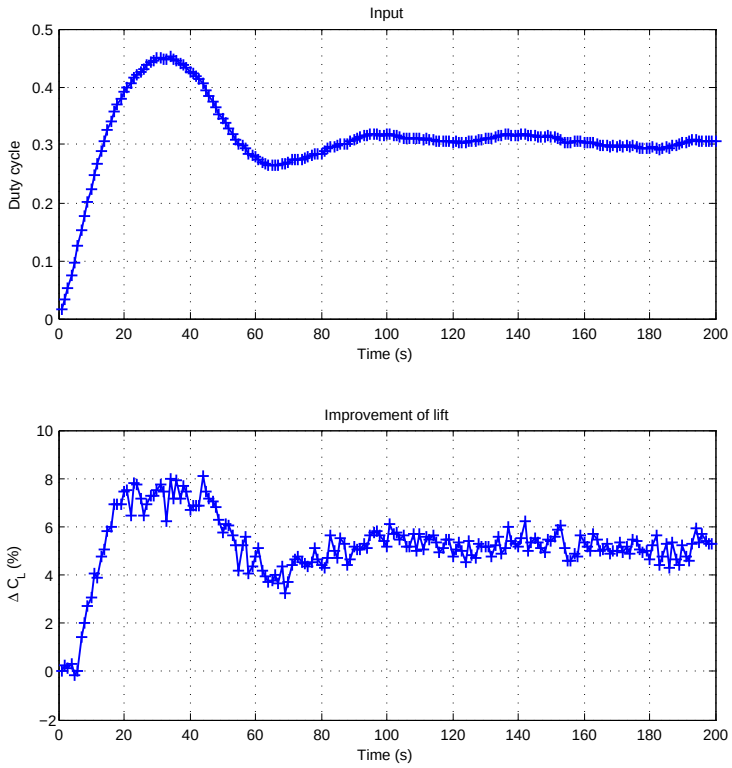


Figure 4.12: Basic PID controller results

Since the derivative term normally increase the over shoot or oscillation of the tracking, a simple PI controller was then tested. Figure 4.13 shows the results of using PI controller, the converge speed was slight slow but there was no overshoot and oscillation in the tracking.

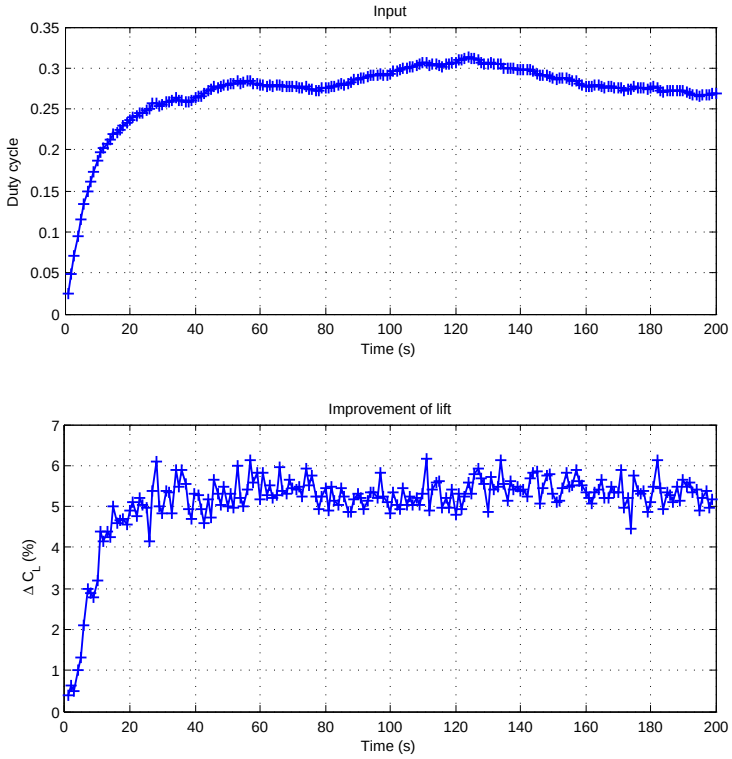


Figure 4.13: Basic PI controller results

### Iterative learning controller

Iterative learning control (ILC) methods were implemented and tested. Since ILC needs the action to operate repeatedly, a trial of 2 seconds or 5 seconds was set. A shorter trial would result in faster response, however, a longer trial could provide better stability as the average measurement over longer period was more accurate. A reference signal was generated by using the open loop results as shown in Figure 4.14.

The basic proportional type (P-type) ILC was tested and the optimal ILC was tested as well. Basically P-type can be describe as:

$$u_{k+1} = u_k + L \cdot e_k \tag{4.2}$$

$$e_k = r - y_k \tag{4.3}$$

where $k$ denotes the iteration number (or trial number), $u_k, y_k, e_k$ are the input, output and tracking error for the $k^{th}$ trial, respectively. $r$ denotes the reference signal. $L$ is the proportional learning gain. The output in this case was the pressure distribution. Figure 4.15 shows the control input and lift improvement over 100 trials using different learning

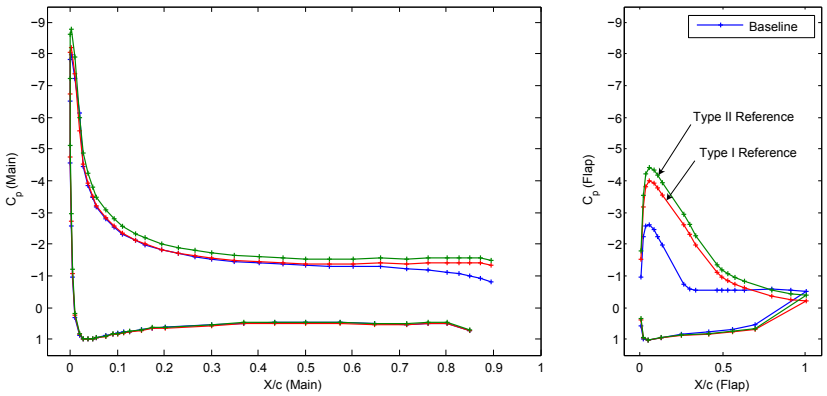


Figure 4.14: Reference signal for the ILC algorithms

gains. The zoomed in section of the figure shows the difference of varying learning gains.

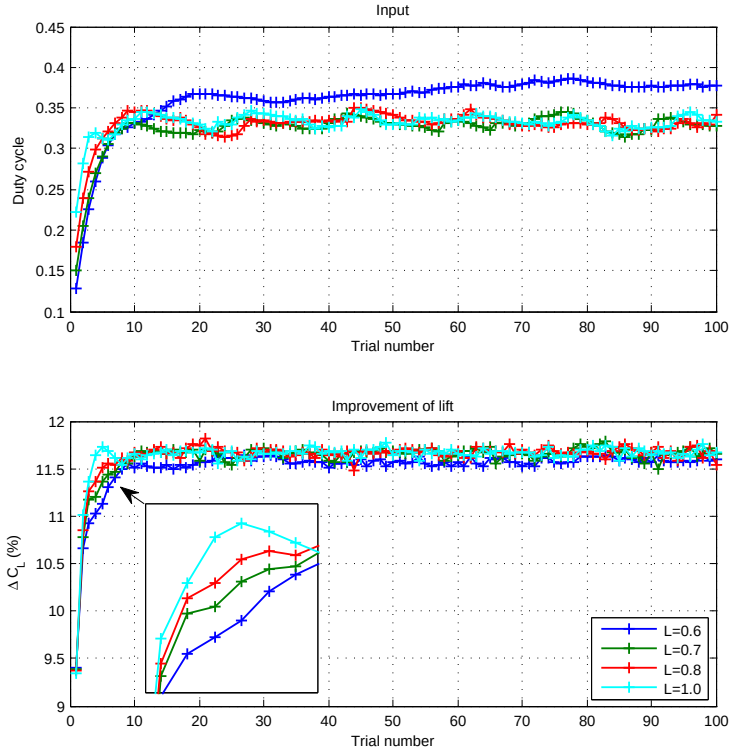


Figure 4.15: Basic P-type ILC results

An optimal learning control algorithms was implemented by using an extended reference signal which is beyond the reach of actuator can do. In this case, the algorithm was trying to find the optimal control input

$$u_{k+1} = u_k + L \cdot \text{sgn}(\frac{\Delta y_k}{\Delta u_k}) \cdot e_k \tag{4.4}$$

$$e_k = r' - y_k \tag{4.5}$$

where $\Delta u_k = u_k - u_{k-1}$ and $\Delta y_k = y_k - y_{k-1}$ and $r'$ was the extended reference and $r' = a \cdot r$ where $a$ is a scalar and $a > 1$. Figure 4.16 shows the results of using optimal ILC with the extended reference.

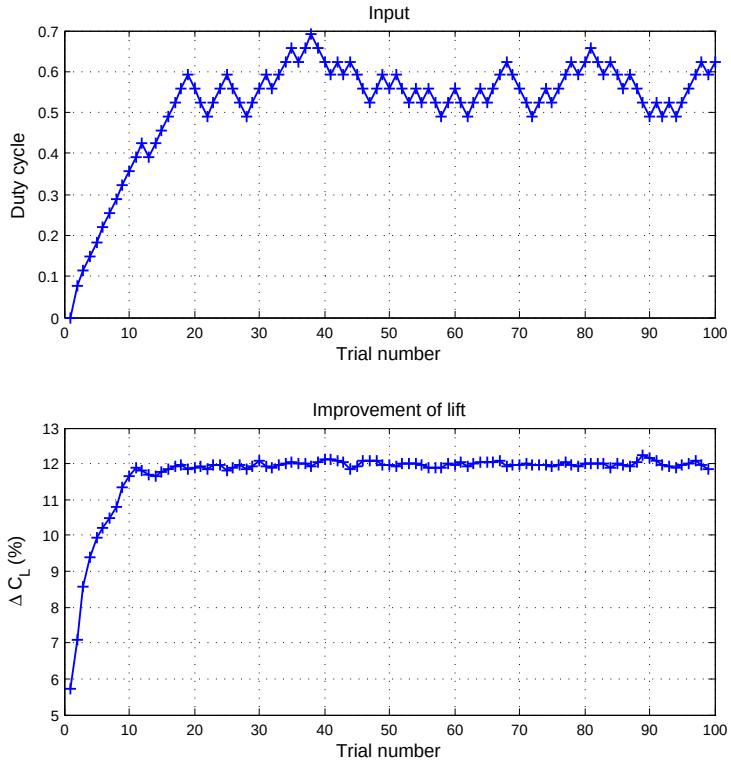


Figure 4.16: Optimal ILC results with extended reference

Figure 4.17 shows the comparison of the using basic ILC and optimal ILC with extended reference. As the basic algorithm used the reference from the open loop results, the improvement would stay at the set point. While the optimal ILC could further improve the performance to reach the optimum result.

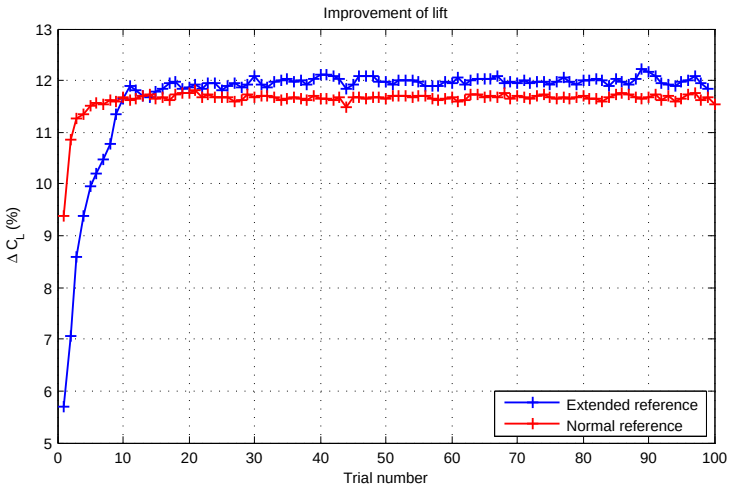


Figure 4.17: Comparison of the optimal ILC and basic P-type ILC

## 4.2 Second wind tunnel tests

This section contains the results of the second wind tunnel test on the mid-scale F15 model (Task 6.3).

In the second wind tunnel test entry, an iterative learning optimisation algorithm was designed. Open loop tests were completed initially to collect the performance data. A 2D model function was then fitted by using surface fitting tools (locally weighted scatter-plot smoothing) and the model was applied in a model based iterative learning optimization algorithm.

### 4.2.1 Control system design and modelling

There are a number of parameters could be varied during the test, including the actuation frequency, the duty cycle, the phase delay and the pressure. As previous wind tunnel experimental results show that tuning variables such as actuation frequency $f$ or the duty cycle $DC$, the performances vary [9]. The overall performance i.e. lift enhancement $\Delta C_L$ and the control inputs can be simply modelled by a concave function. Since these parameter can be tuned at the same time. Modelling and optimisation can be therefore extended to a 2-dimensional case.

For a given system described as

$$y = F(u) \tag{4.6}$$

where $F(\cdot)$ is a concave function. An iterative learning algorithm can be designed to update the control input with the given measurement

$$u_{k+1} = u_k + G(y_k)w \tag{4.7}$$

The objective is to find the optimal control input such as

$$u_k \to u^* = \arg\max_{u \in U} F(u) \tag{4.8}$$

#### Iterative learning algorithm

Given any $u_0 \in U$, the iterative learning algorithm can be employed to solve the above problem

$$u_{k+1} = u_k + LF'(u_k) \tag{4.9}$$

where $L$ is the learning gain which needs to satisfy

$$0 < L < \frac{2}{\max_{u \in U} |F''(u)|}$$

The algorithm requires a model of $y = F(u)$ and uses the derivative of the model to obtain the optimum. Unlike the conventional iterative learning control algorithm. This algorithm

does not need a reference signal or tracking error. However, if the feedback of the system is not used in this case. Therefore an extended algorithm using the system output as feedback can be useful if the

Define

$$G(u) = F^2(u)$$

Since $F(u)$ is positive and concave, $F(u)$ and $G(u)$ will share the same maximum at the same control input $u^*$. Given any $u_0 \in U$, the following algorithm can be given

$$u_{k+1} = u_k + 2LF'(u_k)F(u_k) \tag{4.10}$$

This algorithm enables the use of the feedback from system output $y_k = F(u_k)$. Since the modelling of the system cannot be perfect and there will be some uncertainty. The output feedback will make the system more robust.

### The 2-dimensional case

Equation 4.9 and 4.10 give the algorithm for the optimization with one parameter. If two parameters i.e. control input can be tuned at the same time. For a system given as

$$y_k = F(u_{k,1}, u_{k,2})$$

The iterative learning algorithm of 4.10 can be then revised as

$$u_{k+1,1} = u_{k,1} + 2L_1 \frac{\partial F(\cdot)}{\partial u_{k,1}} F(u_{k,1}, u_{k,2}) \tag{4.11}$$

$$u_{k+1,2} = u_{k,2} + 2L_2 \frac{\partial F(\cdot)}{\partial u_{k,2}} F(u_{k,1}, u_{k,2}) \tag{4.12}$$

When the control inputs were duty cycle, the following constraint needs to be applied.

$$u_k = \begin{cases} 1, & u_k > 1 \\ u_k, & 0 \leq u_k \leq 1 \\ 0, & u_k < 0 \end{cases}$$

### System modelling

The system modelling was completed by using open loop tests. The open loop tests studied the controller with a series of fixed control inputs. Each test lasted 10 seconds in order to ensure enough data were measured and all the pressure measurements could be averaged.

There are two actuation slot line designed. Each of them can be actuated separately. The first open loop test session was to record the lift coefficients by using 11 duty cycles from 0 to 100% with a step of 10% for each actuation line. The results are shown in Figure 4.18. A fitted model was obtained by using locally weighted scatter-plot smoothing (LOWESS).

In the fitted model, an optimum value could be found in the peak area when duty cycle 1 was around 50% and duty cycle 2 was around 80%.

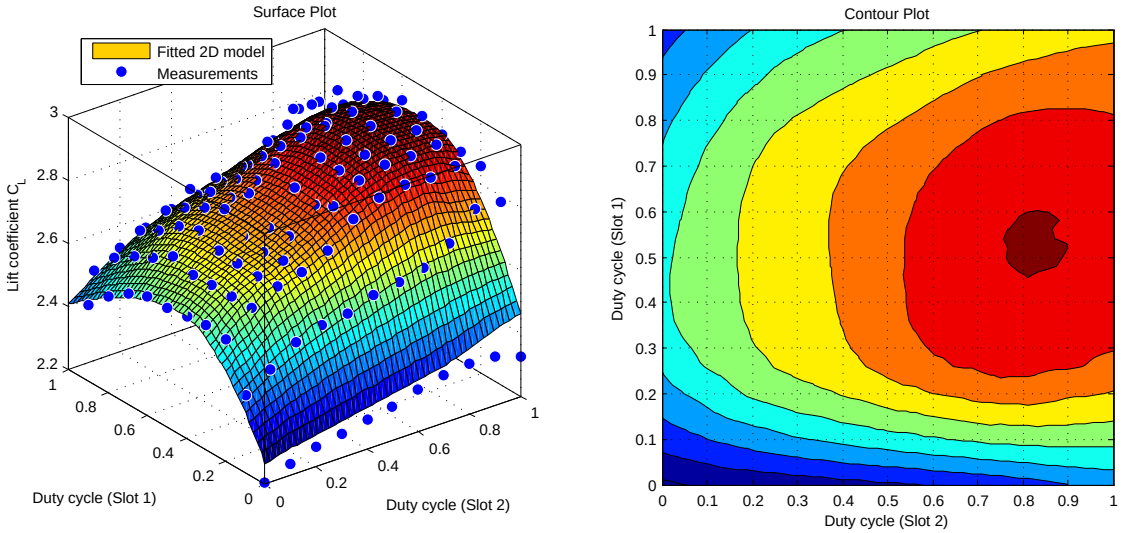


Figure 4.18: Fitted model: duty cycle 1 vs duty cycle 2.

A similar series of tests were conducted for getting the 2D model of varying actuation frequency and duty cycle. 9 steps of frequencies were used from 10 Hz to 150 Hz as well as 11 duty cycles. The same duty cycle was applied to both actuator slot lines in this case. The results and fitted model are shown in Figure 4.19. In this case, optimum performance could be achieved using duty cycle between 70% and 80%, frequency between 60 Hz and 80 Hz.

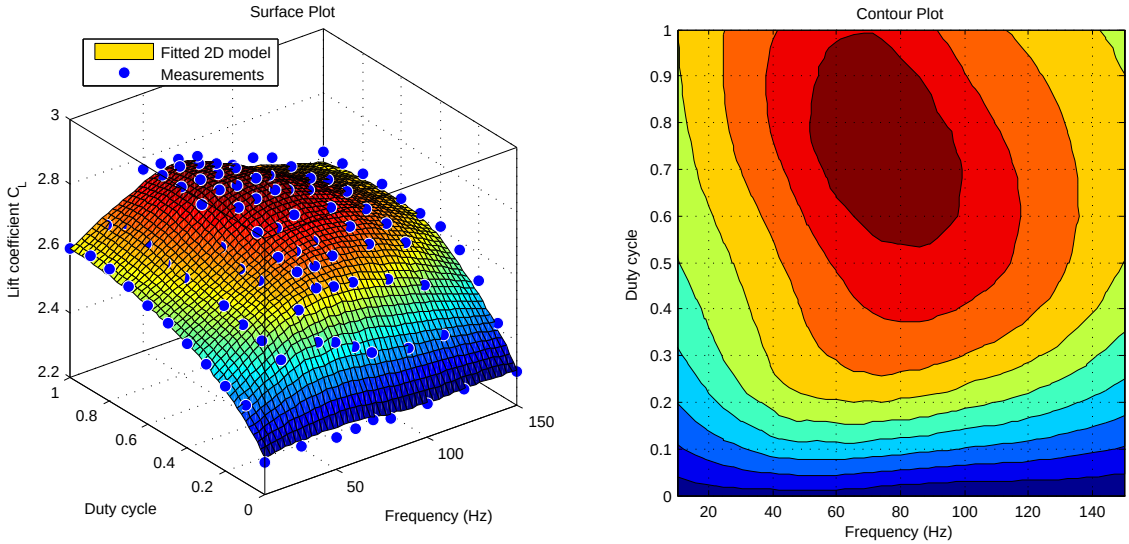


Figure 4.19: Fitted model: duty cycle vs frequency.

### 4.2.2 Wind tunnel experimental results

The wind tunnel experiments included the open loop tests for modelling and verification of actuation, the feedback control tests. The overall performance is estimated by integrating all pressure measurement points along the profile surface. The system repeatedly scanned the surface pressure for a duration of $T$ and updated the control input in between the iterations. By applying the 2D model and the iterative learning algorithm, an optimal performance was achieved.

#### Duty cycle (slot 1) vs duty cycle (slot 2)

Figure 4.20 shows the performance of lift enhancement and the control input for both actuation slot lines. The duty cycles converge to the optimum values as expected. Overall, the controller improved the lift by 18% within less than 5 iteration and the performance was maintained through the tests. The duty cycle of slot line 1 converged to around 52% and the duty cycle of slot line 2 converged to 85.7%.

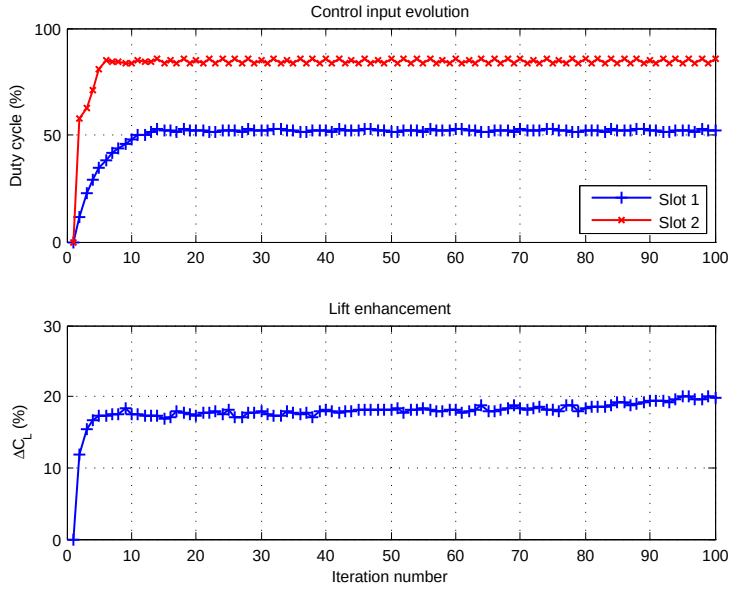


Figure 4.20: Result of optimizing duty cycle 1 vs duty cycle 2 ($L_1 = 0.01$, $L_2 = 0.005$).

The influence of the learning gain $L_1$ and $L_2$ were studied. Figure 4.21 shows 4 sets of results by using 2D model of duty cycle 1 and duty cycle 2. The results indicate that increasing the learning gain values were able to speed up the convergence. However, in terms of the performance when optimal values were approached, smaller gains were able to produce slightly superior results.

#### Duty cycle vs excitation frequency

Figure 4.22 shows the results using the 2D model of the duty cycle and the actuation frequency. In this case, by optimising the actuation frequency and the duty cycle, an

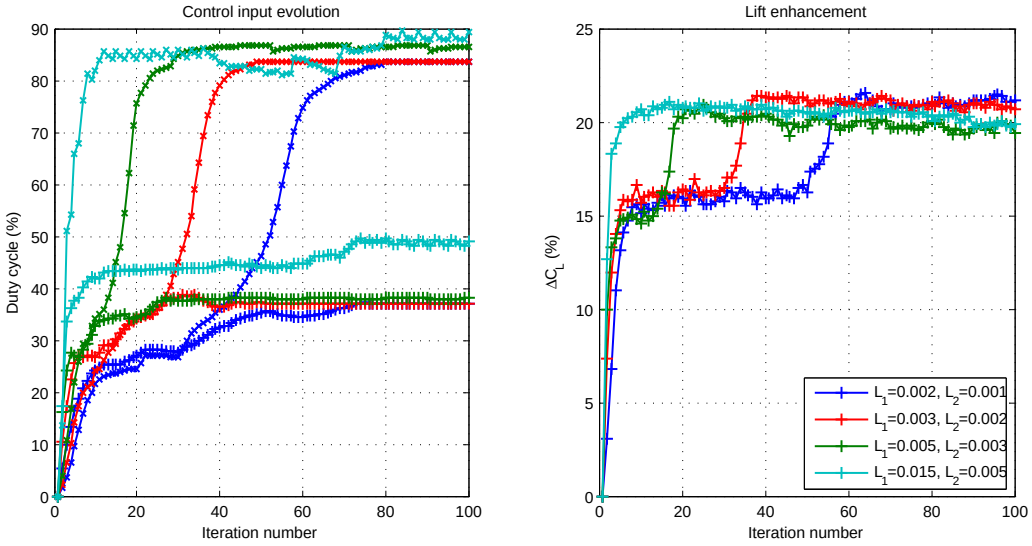


Figure 4.21: The influence of learning gains.

overall improvement of 21% was achieved. The actuation frequency converged to 61.6 Hz while the duty cycle converged to 80.2%.

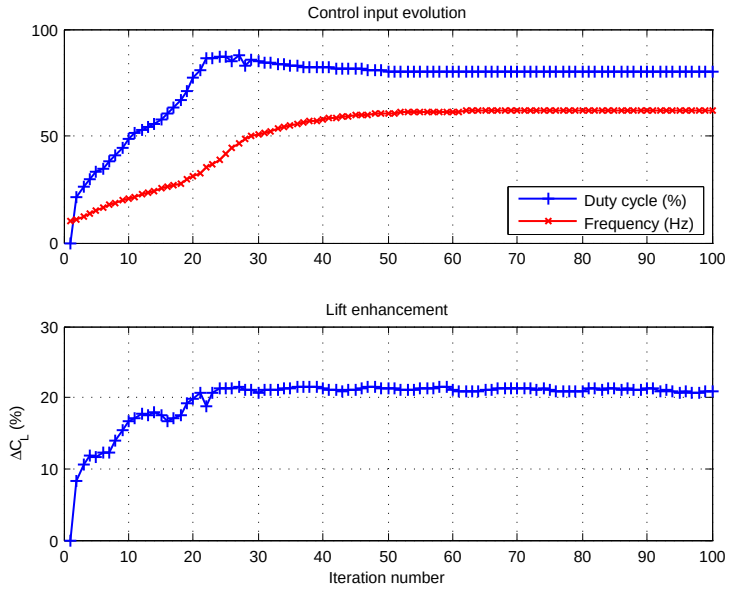


Figure 4.22: Result of optimizing duty cycle vs frequency ($L_1 = 0.01$, $L_2 = 10$).

## 4.3 Flow visualization

### 4.3.1 Particle image velocimetry (PIV) tests

Particle image velocimetry (PIV) tests were conducted to show how the actuation affected the flow. Figure 4.23 shows the results of the flow velocity for the baseline case and the actuated case. These results show the mean velocity field averaged over 100 image pairs.

It shows when the excitation was activate, the mean flow was reattached to the flap.

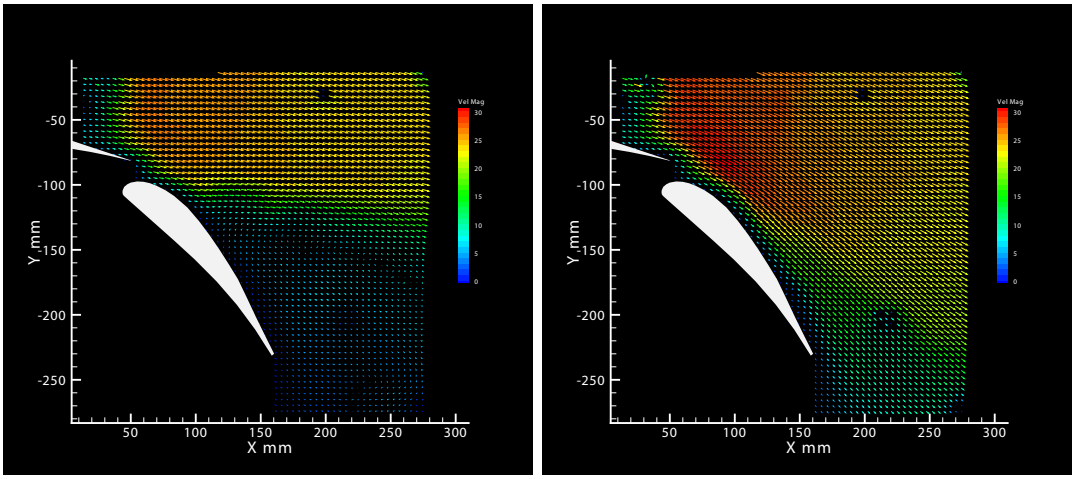


(a) Baseline (b) Actuation

Figure 4.23: PIV results - Velocity magnitude

Figure 4.24 shows the mean turbulence intensity over 100 frames. With the actuation, the turbulence intensity was significantly reduced.

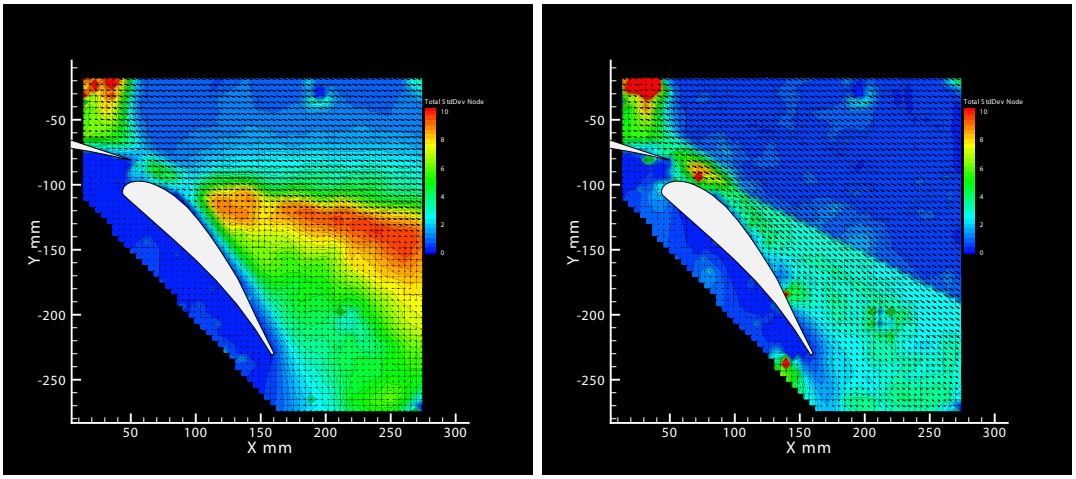


(a) Baseline (b) Actuation

Figure 4.24: PIV results - Turbulence Intensity

Various profiles were taken along the chord of the flap to provide further insight. Due to the increased circulation around the flap with the application of double, the velocity through the gap region is increased. This was evidenced by the increase in the negative pressure peak on the flap. The blowing shows that the blowing filled in the separated wake region. The effect was to displace the velocity downwards towards the flap surface and by filling in the wake, increases the velocity close to the flap surface.

At a profile located at the blowing slot, the velocity showed a little increase. By examining the TKE, there was an increase in the fluctuating velocity close to the blowing slots. This

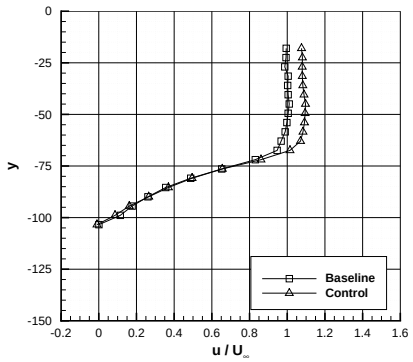


(a) Upstream of actuator.

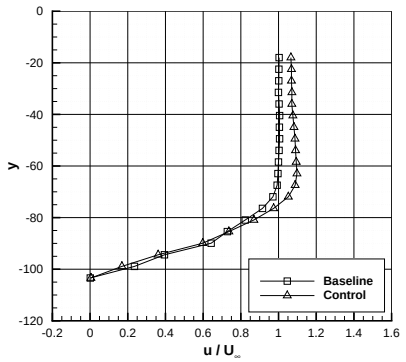


(b) Actuator location.

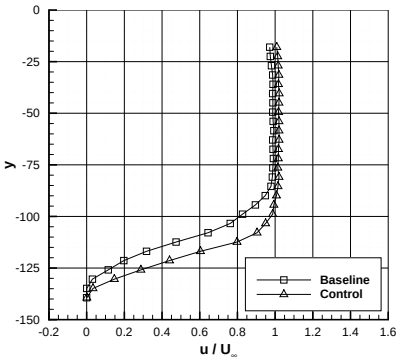


(c) Baseline separation point.

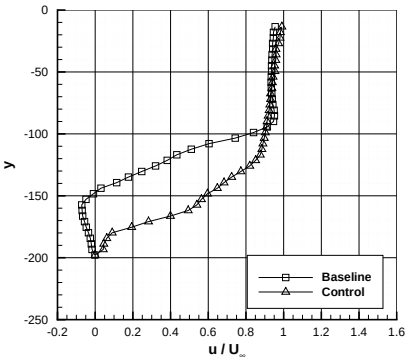


(d) Downstream of actuator.

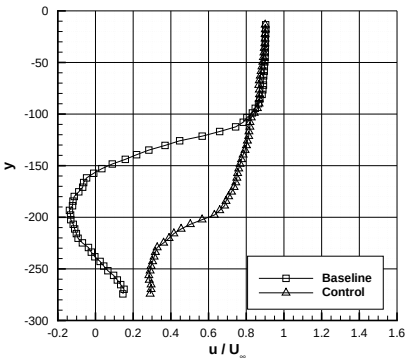


(e) Wake.

Figure 4.25: Mean $u$ velocity profiles.

was due to the unsteady actuation. At downstream profiles, the TKE is reduced since the flow is attached.

By examining the three components of the Reynolds stress tensor, the streamwise fluctuations $u'u'$ were dominated by the shear layer in the separated region above the flap suction surface. With blowing there an increase in this component close to the blowing slot due to the unsteady actuation. The $v'v'$ component was dominated by the unsteady wake in the flap. With blowing this component was increased along the surface of the flap.

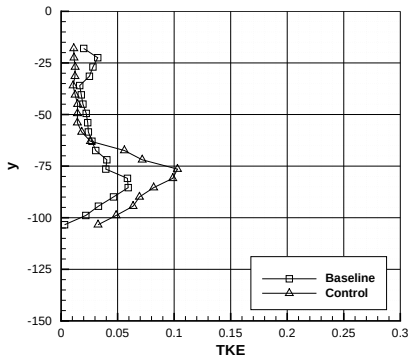


(a) Upstream of actuator.

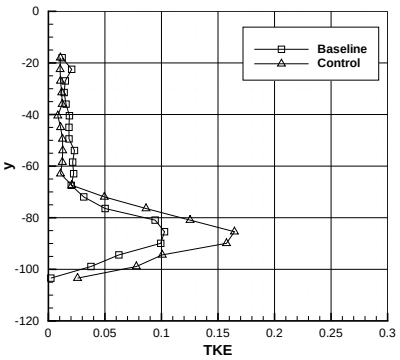


(b) Actuator location.

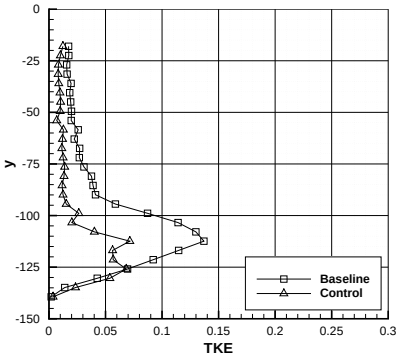


(c) Baseline separation point.

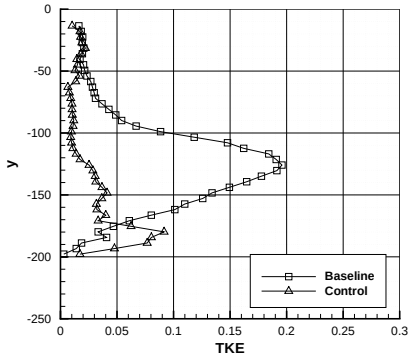


(d) Downstream of actuator.

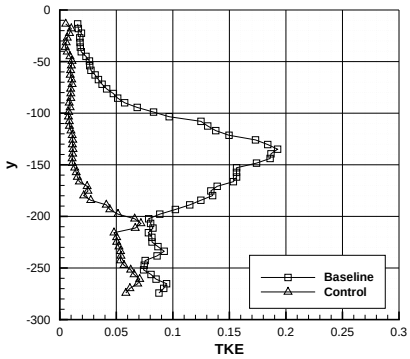


(e) Wake.

Figure 4.26: TKE profiles.

### 4.3.2 Smoke visualisation

Figure 4.27 shows two frames in comparison of the visualized effect of actuation by applying particles such as smoke inside the wind tunnel. Figure 4.27(a) shows the case without actuation. The particles were heavily dispersed and the tufts attached on the flap surface were heading random directions. While in Figure 4.27(b), the particles were concentrated and the tufts were all pointing downstream.

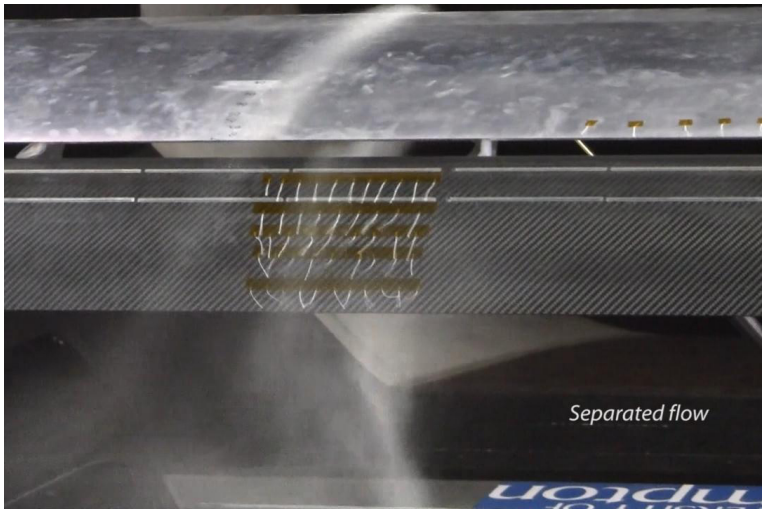


(a) Separated flow

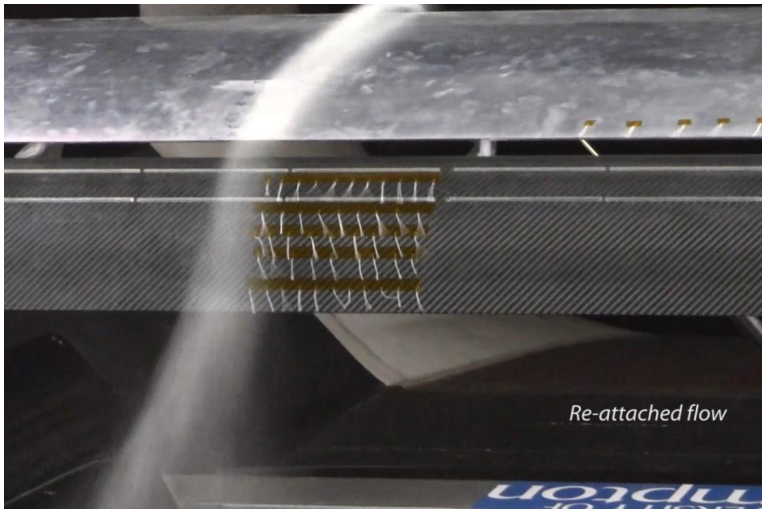


(b) Re-attached flow

Figure 4.27: Visualised effect of the actuation.

# Summary

In this research project, active flow control using pulsed air jets was investigated in order to delay flow separation on a two-element high-lift wing. The actuation was achieved by high pressure compressed air and fast switching solenoid valves. The valves were controlled by a dSPACE ds1006 system with a PC running Matlab/Simulink. A novel position based iterative learning control was developed and applied to active flow separation control. The technique uses surface pressure measurements to update actuation duty cycle iteratively in order to optimise the lift enhancement.

Open loop control tests were performed in order to get data for system modelling and reference generation. Wind tunnel experiments demonstrate that the basic P-type ILC algorithm was able to tracking the given reference and the performance could be maximised by an optimal ILC algorithm with extended reference. Additionally, an iterative learning optimisation algorithm was developed and tested using two two-dimensional models of different variable pairs which were obtained by performing open loop tests. Wind tunnel experiments demonstrated that the method was able to delay flow separation and provide lift enhancement without any reference signal. The control inputs converged to the expected optimal values and an overall lift improvement of approximately 20% was achieved.

The three milestones specified in the Description of Work were completed. This report represents in final deliverable as specified in the Description of Work.

## 5.1 Impact and Dissemination

This research is helpful in terms of fuel efficiency of the air transport. This also has impact on NOx and Carbon emissions indirectly. The technology will be used to help achieve the ACARE 2020 vision. SFWA will work towards the reducing the emissions by 20% and the noise by 5 - 10 dB. Pollution and the reduction in CO2 emissions are also both politically and regulatory important issues. The research is part a continuous stream of research working towards a direction that will further improve the fuel consumption in future aircraft through the use of active flow control.

A paper of the control concept has been submitted to the American Control Conference (ACC) 2013 [10], an annual control conference. A journal version focusing on control

algorithm design and development was published on the International Journal of Control [9]. A conference paper concerning the mid-scale tests will be presented in the summer of 2014.

# Appendix A

# Additional results

The following figures show that the additional results taken from the wind tunnel tests by varying certain learning parameters.

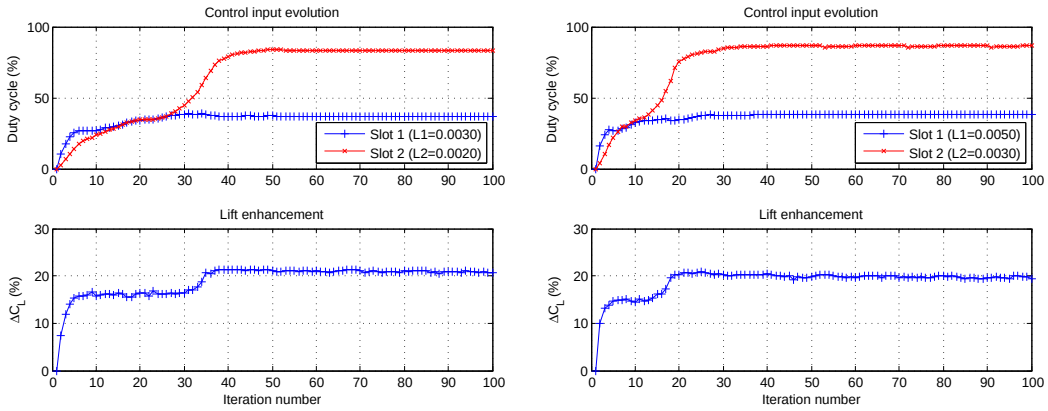


(a)




(b)

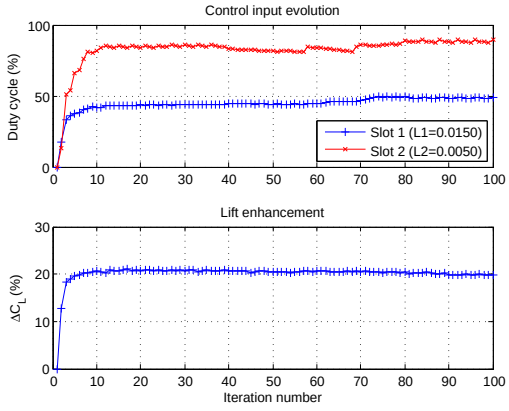


(c)

Figure A.1: Duty cycle (slot 1) vs duty cycle (slot 2)

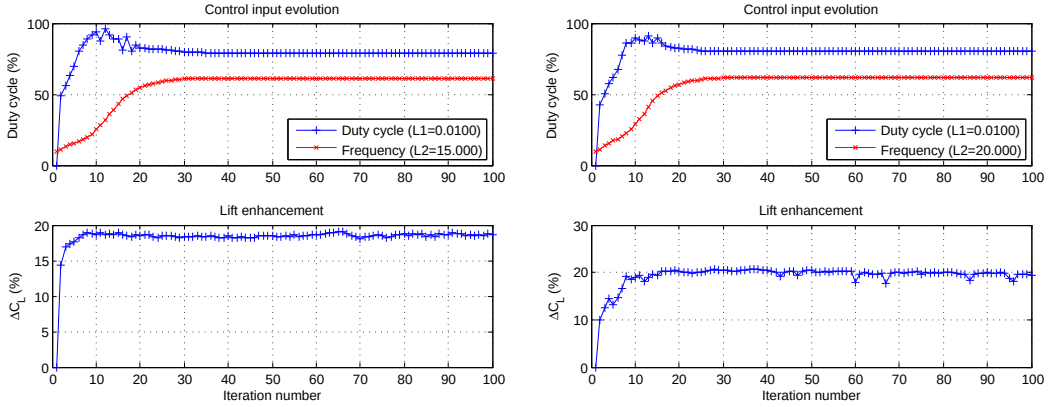


(a) (b)

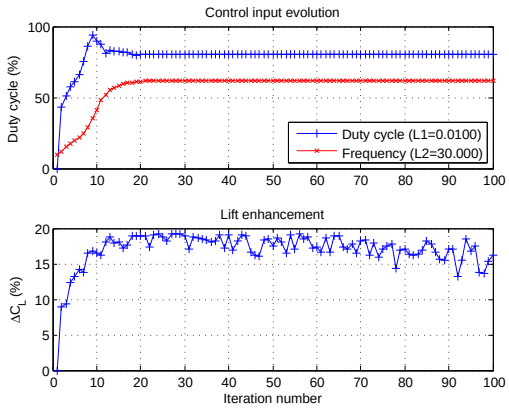


(c)

Figure A.2: Duty cycle vs excitation frequency

# Appendix B

# Mechanical drawings

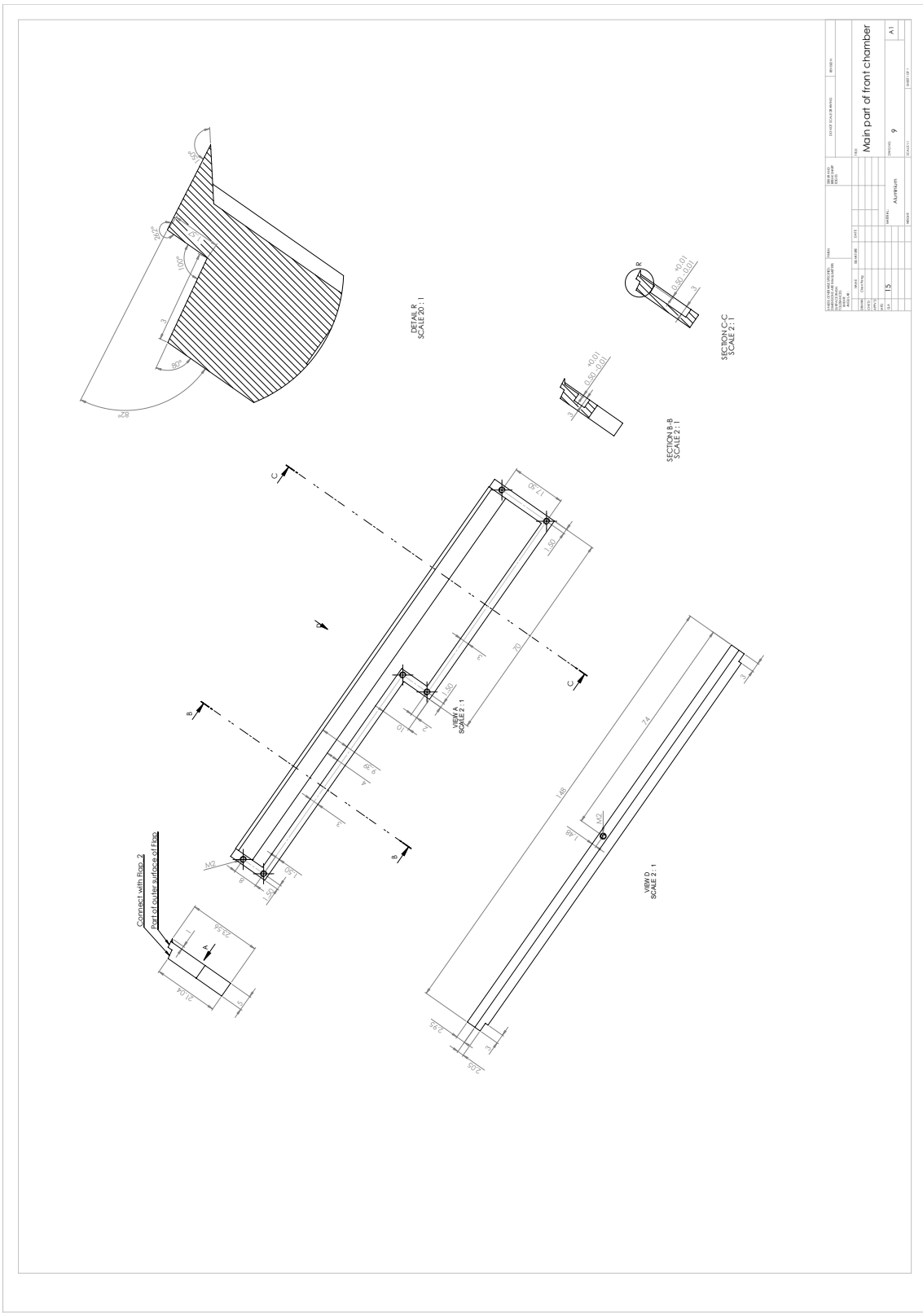


Figure B.1: Design of the front chamber body

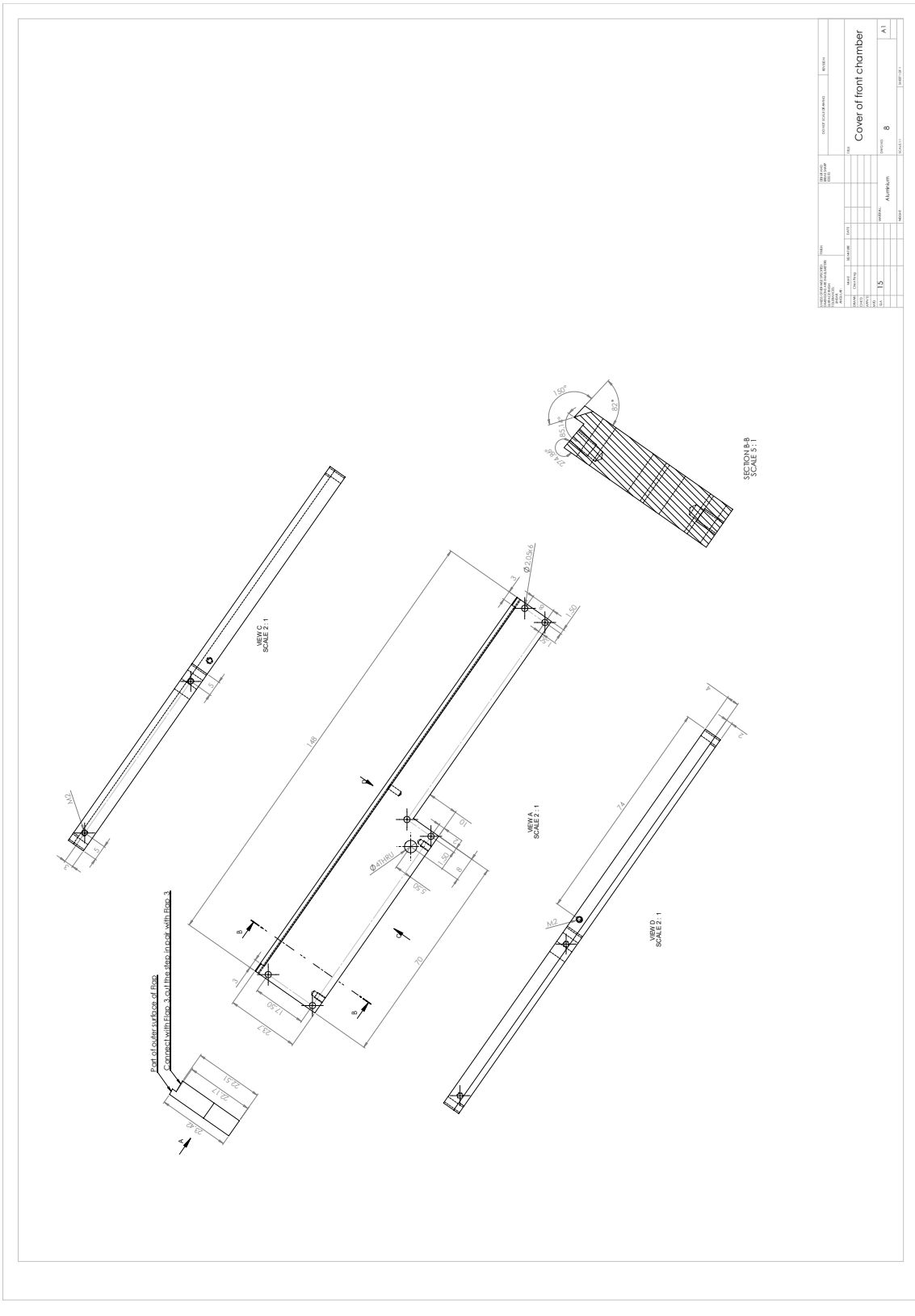


Figure B.2: Design of the front chamber cover

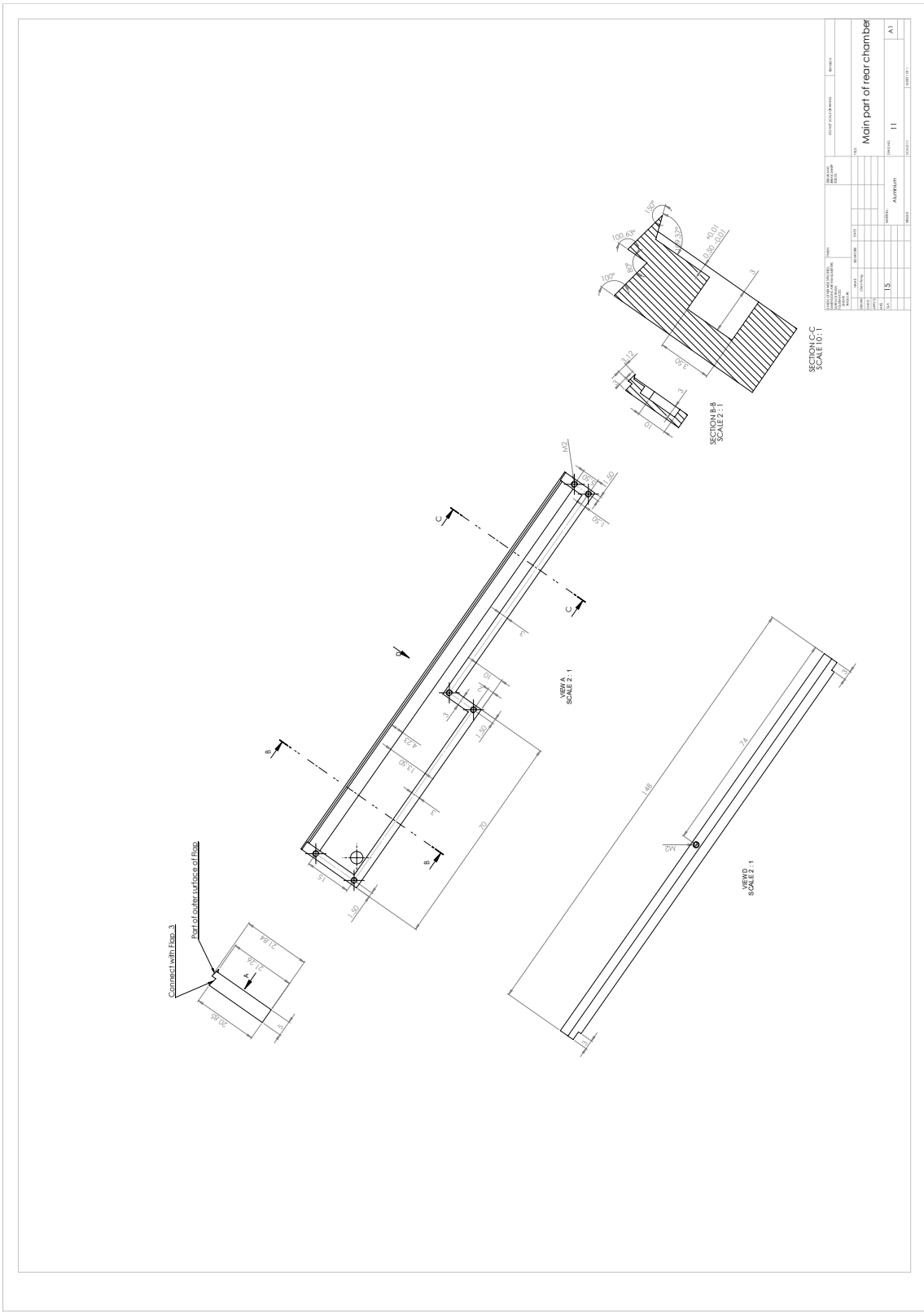


Figure B.3: Design of the rear chamber body

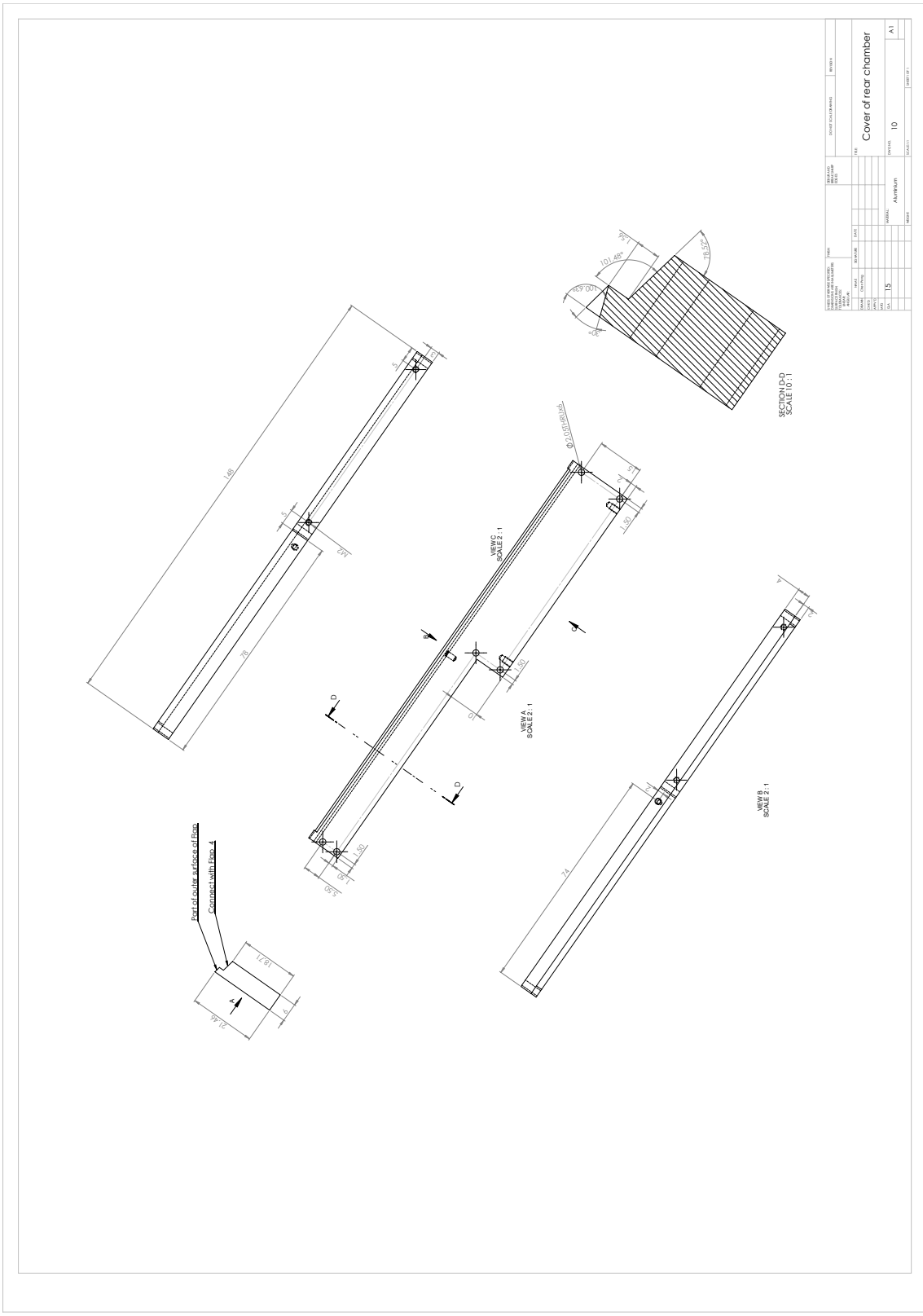


Figure B.4: Design of the rear chamber cover

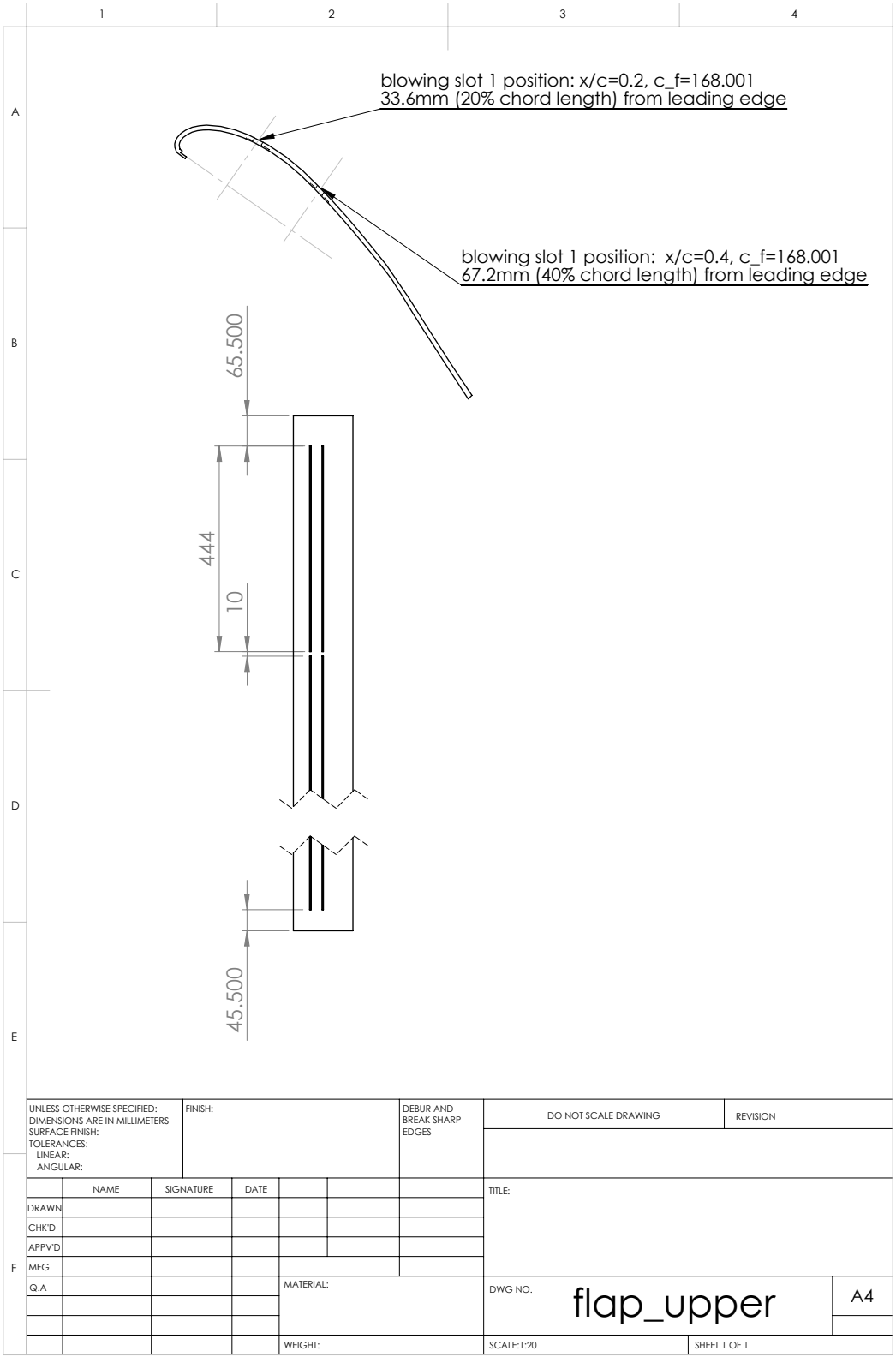


Figure B.5: Design of the flap suction surface

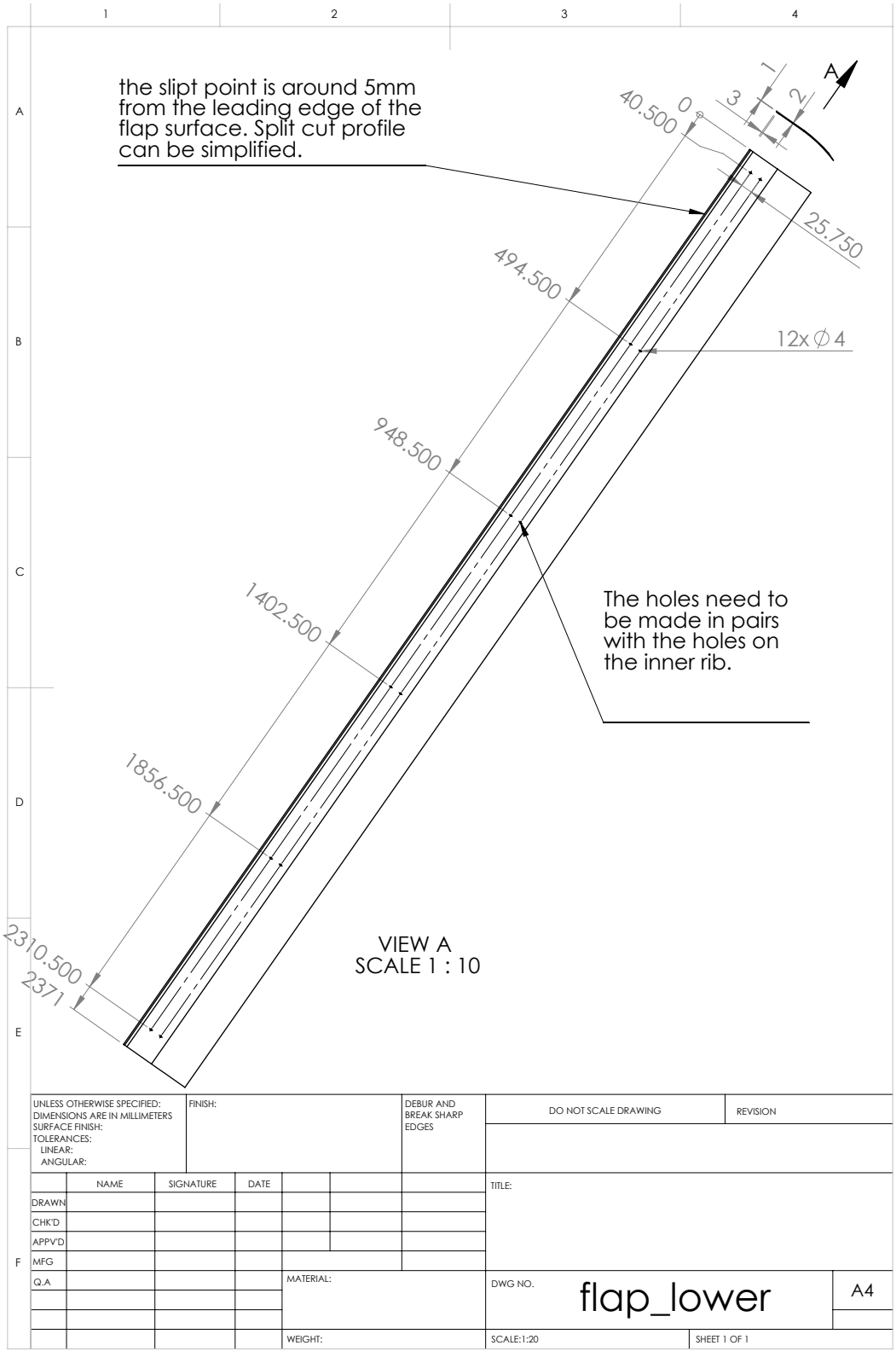


Figure B.6: Design of the flap pressure surface

# Bibliography


[1] "European Aeronautics  A Vision for 2020," *Advisory Council for Aeronautical Research in Europe*, January 2001.

[2] Arimoto, S., Kawamura, S., and Miyazaki, F., "Bettering operations of robots by learning," *Journal of Robotic Systems*, Vol. 1, 1984, pp. 123–140.

[3] Bristow, D. A., Tharayil, M., and Alleyne, A. G., "A Survey of Iterative Learning Control A learning-based method for high-performance tracking control," *IEEE control systems magazine*, Vol. 26, No. 3, 2006, pp. 96–114.

[4] Ahn, H.-S., Chen, Y., and Moore, K. L., "Iterative learning control: brief survey and categorization 1998–2004," *IEEE Transactions on Systems Man and Cybernetics, Part C: Applications and Reviews*, Vol. 37, No. 6, November 2007, pp. 1099–1121.

[5] Wild, J., Wichmann, G., Haucke, F., Peltzer, I., and Scholz, P., "Large-Scale Separation Flow Control Experiments Within the German Flow Control Network," *47th AIAA Aerospace Sciences Meeting*, Orlando, FL, January 2009, pp. AIAA 2009–0530.

[6] Petz, R. and Nitsche, W., "Active Separation Control on the Flap of a Two-Dimensional Generic High-Lift configuration," *Journal of Aircraft*, Vol. 44, No. 3, 2007, pp. 865–874.

[7] Haucke, F., Peltzer, I., and Nitsche, W., "ACTIVE SEPARATION CONTROL ON A SLATLESS 2D HIGH-LIFT WING SECTION," *26th International Congress of The Aeronautical Sciences*, Anchorage, AK, September 2008.

[8] Arimoto, S., Miyazaki, F., Kawamura, S., and Tamaki, S., "Learning control theory for dynamical systems," *Proceedings of the 24th Conference on Decision and Control*, Fort Lauderdale, Florida, 1985, pp. 1375–1380.

[9] Cai, Z., Chen, P., Angland, D., and Zhang, X., "Active Flow Separation Control by a Positional Based Iterative Learning Control with Experimental Validation," *International Journal of Control*, Vol. 87, No. 3, January 2014, pp. 633–641.

[10] Cai, Z., Chen, P., Angland, D., and Zhang, X., "A Position Based Iterative Learning Control Applied to Active Flow Control," *Proceedings of 2013 American Control Conference*, Washington DC, USA, June 2013, pp. 5184–5189.